Neurobiology of Disease 77 (2015) 35–48

Contents lists available at ScienceDirect

Neurobiology of Disease

journal homepage: www.elsevier.com/locate/ynbdi

Functional and structural deficits of the dentate gyrus network coincide with emerging spontaneous seizures in an *Scn1a* mutant Dravet Syndrome model during development

Ming-Shian Tsai [a,1], Meng-Larn Lee [b,1], Chun-Yun Chang [c], Hsiang-Hsuan Fan [d], I-Shing Yu [e], You-Tzung Chen [d], Jhih-Yi You [a], Chun-Yu Chen [a], Fang-Chia Chang [b], Jane H. Hsiao [f], Olga Khorkova [f], Horng-Huei Liou [g], Yuchio Yanagawa [h], Li-Jen Lee [i,j,*], Shu-Wha Lin [a,k,l,**]

[a] Department of Clinical Laboratory Sciences and Medical Biotechnology, National Taiwan University Hospital, College of Medicine, National Taiwan University, Taipei 100, Taiwan
[b] Department of Veterinary Medicine National Taiwan University, Taipei 100, Taiwan
[c] National Institute on Drug Abuse (NIDA)-Intramural Research Program, Baltimore, MD 21224, USA
[d] Graduate Institute of Medical Genomics and Proteomics, National Taiwan University Hospital, College of Medicine, National Taiwan University, Taipei 100, Taiwan
[e] Laboratory animal center, National Taiwan University Hospital, College of Medicine, National Taiwan University, Taipei 100, Taiwan
[f] OPKO Health, Inc., Miami, FL 33137, USA
[g] Department of Neurology, National Taiwan University Hospital, College of Medicine, National Taiwan University, Taipei 100, Taiwan
[h] Department of Genetic and Behavioral Neuroscience, Gunma University Graduate School of Medicine and JST, CREST, Maebashi 371–8511, Japan
[i] Graduate Institute of Anatomy and Cell Biology, National Taiwan University Hospital, College of Medicine, National Taiwan University, Taipei 100, Taiwan
[j] Graduate Institute of Brain and Mind Sciences, National Taiwan University Hospital, College of Medicine, National Taiwan University, Taipei 100, Taiwan
[k] Department of Laboratory Medicine, National Taiwan University Hospital, College of Medicine, National Taiwan University, Taipei 100, Taiwan
[l] Center for Genomic Medicine, National Taiwan University, Taipei 100, Taiwan

ARTICLE INFO

Article history:
Received 21 October 2014
Revised 3 January 2015
Accepted 16 February 2015
Available online 26 February 2015

Keywords:
SCN1A
Dravet syndrome
Epilepsy
Mouse model

ABSTRACT

Dravet syndrome (DS) is characterized by severe infant-onset myoclonic epilepsy along with delayed psychomotor development and heightened premature mortality. A primary monogenic cause is mutation of the *SCN1A* gene, which encodes the voltage-gated sodium channel subunit $Na_v1.1$. The nature and timing of changes caused by *SCN1A* mutation in the hippocampal dentate gyrus (DG) network, a core area for gating major excitatory input to hippocampus and a classic epileptogenic zone, are not well known. In particularly, it is still not clear whether the developmental deficit of this epileptogenic neural network temporally matches with the progress of seizure development. Here, we investigated the emerging functional and structural deficits of the DG network in a novel mouse model ($Scn1a^{E1099X/+}$) that mimics the genetic deficit of human DS. $Scn1a^{E1099X/+}$ (Het) mice, similarly to human DS patients, exhibited early spontaneous seizures and were more susceptible to hyperthermia-induced seizures starting at postnatal week (PW) 3, with seizures peaking at PW4. During the same period, the Het DG exhibited a greater reduction of $Na_v1.1$-expressing GABAergic neurons compared to other hippocampal areas. Het DG GABAergic neurons showed altered action potential kinetics, reduced excitability, and generated fewer spontaneous inhibitory inputs into DG granule cells. The effect of reduced inhibitory input to DG granule cells was exacerbated by heightened spontaneous excitatory transmission and elevated excitatory release probability in these cells. In addition to electrophysiological deficit, we observed emerging morphological abnormalities of DG granule cells. Het granule cells exhibited progressively reduced dendritic arborization and excessive spines, which coincided with imbalanced network activity and the developmental onset of spontaneous seizures. Taken together, our results establish the existence of significant structural and functional developmental deficits of the DG

Abbreviations: AIS, axon initial segment; AHP, afterhyperpolarization; CA1, cornu ammonis 1; CA3, cornu ammonis 3; DG, dentate gyrus; DS, Dravet syndrome; EPSC, excitatory postsynaptic current; ES cell, embryonic stem cell; GABA, gamma-aminobutyric acid; GAD, glutamate decarboxylase; HIS, hyperthermia-induced seizure; IPSC, inhibitory postsynaptic current; KI, knock-in; PB, phosphate buffer; PD, postnatal day; PPR, p aired-pulse ratio; PV, parvalbumin; PW, postnatal week; PSC, postsynaptic current; SCN1A, sodium channel type I α subunit; WT, wild type.

* Correspondence to: L.-J. Lee, Graduate Institute of Anatomy and Cell Biology, College of Medicine, National Taiwan University, No. 1, Section 1, Ren-Ai Rd., 100 Taipei, Taiwan.
** Correspondence to: S.-W. Lin, Department of Clinical Laboratory Sciences and Medical Biotechnology, College of Medicine, National Taiwan University, No. 7, Chung-San S. Rd., 100 Taipei, Taiwan. Fax: +886 2 2381 7083.
E-mail addresses: ljlee@ntu.edu.tw (L.-J. Lee), mtshuwha@ntu.edu.tw (S.-W. Lin).
[1] These authors contributed equally.
Available online on ScienceDirect (www.sciencedirect.com).

http://dx.doi.org/10.1016/j.nbd.2015.02.010

network and the temporal correlation between emergence of these deficits and the onset of seizures in Het animals. Most importantly, our results uncover the developmental deficits of neural connectivity in Het mice. Such structural abnormalities likely further exacerbate network instability and compromise higher-order cognitive processing later in development, and thus highlight the multifaceted impacts of *Scn1a* deficiency on neural development.

Introduction

Dravet syndrome (DS), which is primarily caused by genetic mutation in the sodium channel-encoding gene *SCN1A*, is a neurodevelopmental disorder. The typical symptoms of DS include severe fever-induced febrile epilepsy and generalized seizures during infancy (Harkin et al., 2007). The frequency and severity of seizures grow worse over time, concomitantly with the development of other seizure types (Harkin et al., 2007).

More than two-thirds of DS patients carry a loss-of-function mutation in *SCN1A*, which encodes the α subunit of the voltage-gated sodium channel $Na_v1.1$. In rodents, the central expression of $Na_v1.1$ becomes detectible starting at PW2 and plateaus by PW4 (Gazina et al., 2010; Ogiwara et al., 2007). This time frame coincides with massive activity-dependent dendritic and spine remodeling in the hippocampus and other cortical areas during development (Gomez-Di Cesare et al., 1997; Miller, 1981). $Na_v1.1$ is predominately expressed in the axon and soma of fast-spiking parvalbumin (PV)-positive (PV(+)) interneurons (Ogiwara et al., 2007; Wang et al., 2011), with some expression observed in a small fraction of CaMKII -expressing excitatory neurons in the hippocampus and neocortex (Dutton et al., 2012). Despite being expressed in different neuron types, heterozygous *Scn1a* mutations appear to selectively affect interneurons (Cheah et al., 2012; Dutton et al., 2012; Tai et al., 2014). Functionally, $Na_v1.1$ is essential for gating action potential (AP) initiation, being one of the major sodium channels residing in the axon initial segment (AIS, Duflocq et al., 2008; Ogiwara et al., 2007). Anatomically, $Na_v1.1$-expressing interneurons appear to play a more significant role in specific brain areas, such as the dentate gyrus (DG) and cortical areas, as these areas suffer a much greater loss of $Na_v1.1$-expressing gamma-aminobutyric acid (GABA)ergic neurons in *Scn1a* loss-of-function mouse models (Cheah et al., 2012; Han et al., 2012).

In currently available *Scn1a*-deficient DS mouse models (all DS models mentioned are referring to those with *Scn1a* mutations, unless otherwise specified), the frequency of spontaneous seizures primarily peaks by PW4 (Cheah et al., 2012; Kalume et al., 2013; Ogiwara et al., 2007; Yu et al., 2006). The peak of spontaneous seizures matches the developmental expansion of $Na_v1.1$ expression. Electrophysiological recording in animal models that carry *Scn1a* mutation suggests that epileptic activity during hyperthermia-induced seizures (HISs) might initiate in the hippocampus (Ohno et al., 2011; Liautard et al., 2013; but see Dutton et al., 2012). While most of the hippocampal-related research in *Scn1a* models focuses on the hippocampal CA1 area, the pathological consequence of *Scn1a* dysfunction in the DG, a core area for gating major excitatory input to hippocampus, has been largely overlooked. Moreover, there is still no systematic validation of the temporal correlation between the developmental onset of seizures and the emerging developmental deficit of an epileptogenic network. In the present study, we aimed to delineate the impact of $Na_v1.1$ deficiency on the developing DG network in a new DS mouse model harboring an *Scn1a* mutation ($Scn1a^{E1099X}$) that is identical to one found in a subset of DS patients. Our results show that $Na_v1.1$ deficiency results in progressively impaired structural and functional development of DG granule cells. Furthermore, our findings strongly support the idea that the onset of spontaneous seizures is precisely correlated with expansion of $Na_v1.1$-expressing GABAergic neurons and emergence of these structural and functional deficits in DG network during development.

Materials and methods

Generation and maintenance of $Scn1a^{E1099X}$ knock-in mice

All of the animal experiments were performed in accordance with guidelines established by the Institutional Animal Care and Use Committee of the National Taiwan University College of Medicine. A targeting vector, pL253-*Scn1a*, was developed based on the recombineering method and constructed following previously described procedures (Liu et al., 2003). The homologous arm was a 15-kb genomic DNA fragment comprising exons 10–17 of the *Scn1a* gene from a 129/Sv background (bMQ419a06, purchased from Source BioScience, Nottingham, UK). To insert the TAG stop codon, a 600-bp fragment containing exon 17 and its upstream and downstream sequences was first subcloned into *Not*I/*Bam*HI sites of pL452, which harbors a neomycin-resistance cassette surrounded by two *lox*P sites. This changed the wild type GAG codon (glutamic acid, E) at position 1099 to TAG (X), generating the desired E1099X mutation. The resulting plasmid, pL452-E1099X, which carried E1099X and the neo-2-*lox*P cassette, was inserted into pL253-*Scn1a* by recombineering to generate the pL253-*Scn1a*-E1099X plasmid. The plasmid was linearized by *Not*I digestion and electroporated into R1 hybrid embryonic stem (ES) cells (129X1 x 129S1). Successfully targeted ES cell clones were isolated and identified by Southern blotting (see Fig. 1 legend). A Cre-expressing plasmid was used to excise the Neo cassette from the correctly targeted ES cell clones (Huang et al., 2011). After transfection, the surviving individual ES cell clones were isolated and screened by PCR using primers AU (5′-AGGGAGATGAATGCCAAAGC-3′) and BD (5′-GACAATTGGTAGGGAGCACT-3′) in a PCR reaction with the following conditions: 95 °C for 2 min, followed by 40 cycles of 95 °C for 30 sec, 55 °C for 1 min and 72 °C for 1 min, and a final extension at 72 °C for 7 min. The PCR reaction yielded a 359-bp amplicon from the wild-type (WT) allele and a 459-bp amplicon from the knock-in (KI) allele. Chimeric mice were generated by injecting the resulting KI ES cell clones into C57BL/6JNarl blastocysts (Chen et al., 2012). Germ-line transmission of the $Scn1a^{E1099X}$ allele was achieved by breeding chimeric mice with C57BL/6JNarl female mice and was verified by the genotyping, sequencing, and Southern blotting of genomic DNA from the offspring. $Scn1a^{E1099X}$ allele in a 129 background was generated by mating the male chimeric mice with 129 female mice (129S2/SvPasCrl; Charles River, L'Arbresle Cedex, France). Mice in the B6:129 N2 (~75%/25%) genetic background were used for the experiments, unless otherwise indicated. To generate $Gad1^{GFP/+}$:$Scn1a^{E1099X/+}$ animals, $Scn1a^{E1099X/+}$ mice in a 129 background were crossed with $Gad1^{GFP/+}$ mice in a B6 background (kindly provided by Dr. Yuchio Yanagawa) (Tamamaki et al., 2003). The resulting $Gad1^{GFP/+}$:$Scn1a^{+/+}$ and $Gad1^{GFP/+}$:$Scn1a^{E1099X/+}$ mice thus carry a mixed B6:129 (50%/50%) background.

Immunoblot analysis

Whole brains were collected from $Scn1a^{+/+}$ (WT), $Scn1a^{E1099X/+}$ (Het), and $Scn1a^{E1099X/E1099X}$ (Homo) mice (3 mice for each genotype) at postnatal day (PD) 14, and hippocampi were dissected from WT and Het mice (5 mice for each age group) at PW3, PW4, and PW6. The samples were homogenized in a protein extraction reagent (T-per, Thermo Fisher Scientific, Waltham, MA, USA) containing 1% protease inhibitor (Sigma-Aldrich, St Louis, MO, USA). The total protein concentration was determined using a Pierce BCA protein assay kit (Thermo

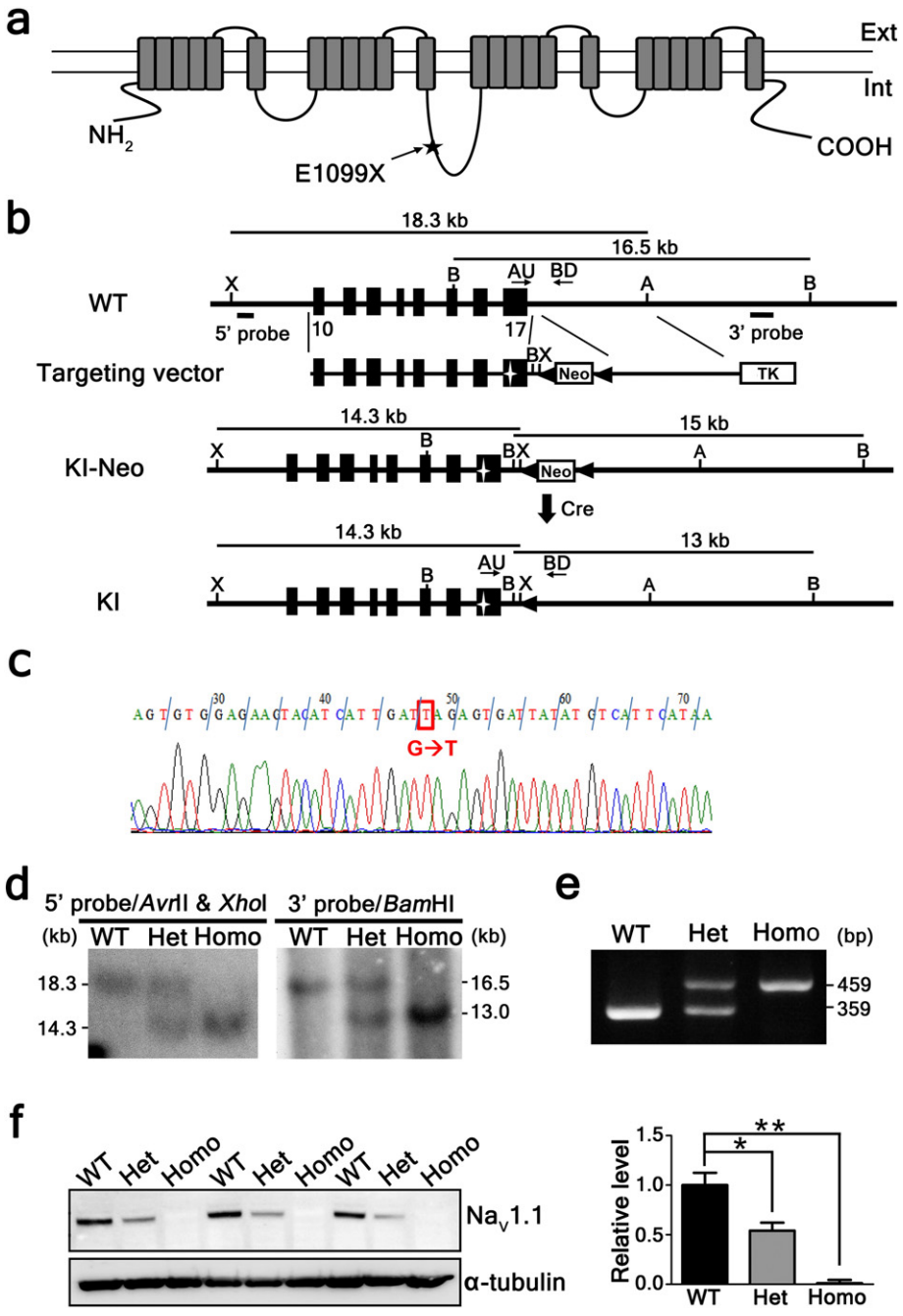

Fig. 1. Generation of *Scn1a*^{E1099X} mice. a. Location of E1099X on the SCN1A protein. E1099X is located in the linker between domains 2 and 3. Ext, extracellular; Int, intracellular. b. Gene-targeting strategy for generating the *Scn1a*^{E1099X} allele. WT, wild type; KI, knock-in; filled boxes, exons; filled box with star, E1099X in exon 17; filled triangles, *lox*P; Neo, neomycin resistance gene; TK, thymidine kinase gene; Cre, Cre recombinase; A, *Avr*II site; B, *Bam*HI site; X, *Xho*I site; AU and BD, primers for PCR genotyping. c. Sequence verification of the E1099X mutation. Genomic DNA sequencing from *Scn1a*^{E1099X} mouse tail confirmed the presence of premature stop codon (GAG→TAG; E1099X) in the newly generated animals. d. *Scn1a*^{E1099X} offspring were genotyped by Southern blot. Tail DNA was digested with *Avr*II plus *Xho*I (for 5′ probe) or *Bam*HI (for 3′ probe). With the 5′ probe, the enzyme digestion products of WT and KI alleles are 18.3 kb and 14.3 kb, respectively. With the 3′ probe the digestion products are 16.5 kb (WT) and 13 kb (KI). e. The genotypes of *Scn1a*^{E1099X} allele were verified using PCR genotyping with primers AU and BD. WT amplicon: 359 bp; KI amplicon: 459 bp. f. The protein expression level of Na$_v$1.1 in all *Scn1a*^{E1099X} allele genotypes. The protein lysates were extracted from the whole brain of WT, Het, and Homo mice at PD14, and were analyzed by immunoblotting with an anti-Na$_v$1.1 antibody. The expression level was normalized to α-tubulin (3 mice for each genotype).

Fisher Scientific). The protein samples were mixed with 4× NuPAGE lithium dodecyl sulfate sample buffer (Invitrogen, Grand Island, NY, USA) and 4× NuPAGE reducing reagent (Invitrogen). The samples were separated on a NuPAGE Novex Tris-acetate 3-8% gel (Invitrogen) and electrotransferred onto a polyvinylidene fluoride (PVDF) membrane. The blots were probed with primary antibodies against Na$_v$1.1 (1:300; Millipore, Billerica, MA, USA), Na$_v$1.2 (1:500; Millipore), Na$_v$1.3 (1:200; Millipore), Na$_v$1.6 (1:500; Alomone Labs, Jerusalem, Israel), and α-tubulin (1:10,000; Sigma). The primary antibodies were recognized by horseradish peroxidase (HRP)-conjugated anti-mouse IgG or anti-rabbit IgG secondary antibodies (both 1:10,000; Millipore). The secondary antibodies were later detected by Immobilon Western Chemiluminescent HRP substrate (Millipore) or SuperSignal West Femto Maximum Sensitivity substrate (Thermo Fisher Scientific). The signal was collected and quantified using Multi Gauge v3.0 software (Fujifilm, Tokyo, Japan) and normalized to the expression of α-tubulin.

Electroencephalography

Mice (3 mice for each genotype) at PW8-PW12 were used for electroencephalography (EEG) studies. EEG electrodes were put in direct contact with the cortex while the animals were under ketamine/xylazine anesthesia. Recordings were collected using a V75-01 amplifier (Colbourn Instruments, Lehigh Valley, PA, USA) and band-pass filtered between 0.1 and 40 Hz. Digitized EEG waveforms were stored as binary computer files for subsequent analysis. Post-acquisition determination of seizure events in EEG recordings was performed by visual scoring (Jou et al., 2013) using AxoScope 10 software (Molecular Devices, Sunnyvale, CA, USA).

Video recording and seizure analysis

WT and Het mice (5 WT mice and 29 Het mice) were continuously and individually video-monitored in their home cages from PD20 to PD25. Seizure severity was scored based on Racine stages (Racine, 1972): 0, no response; 1, mouth and facial movement; 2, head nodding; 3, forelimb clonus; 4, forelimb clonus with rearing; and 5, generalized tonic-clonic seizures and falling.

Seizure induction by hyperthermia

The body temperatures of WT and Het mice (20 mice for each age group) at PW3-PW5 and PW16-PW20 were elevated by 0.5 °C steps every 2 min, with monitoring performed using a rectal temperature probe (Cheah et al., 2012). The mice were video-recorded until a seizure was observed. The rectal temperature at which a seizure (Racine stage 3 or higher) was induced was defined as the threshold temperature of HIS.

Measurement of hippocampal GABA concentration

Hippocampi were dissected from WT and Het male mice at PW3 (4 mice for each genotype) and PW4 (11 mice for each genotype). GABA concentrations were measured using a GABA Research ELISA kit (Labor Diagnostika Nord, Nordhorn, Germany) according to the manufacturer's instructions. Briefly, dissected hippocampi were homogenized separately and each supernatant was used to measure the GABA level by using the GABA ELISA kit. The total protein concentration was determined using a Pierce BCA protein assay kit (Thermo Fisher Scientific). The hippocampal GABA concentration was normalized to the total protein concentration.

Immunohistochemistry and quantification

Male mice (3 mice for each age group) at PW3 and PW4 were perfused with normal saline followed by 4% paraformaldehyde in 0.1 M phosphate buffer (PB). Whole brains were isolated and post-fixed in the same fixative for 3 hr at 4 °C, and then embedded in paraffin. Coronal sections (5 μm) were cut, deparaffinized, and incubated in 10 mM citrate buffer for epitope retrieval. Tissue sections were immersed in 0.1% Triton X-100 in PBS and blocked with Rodent-block M (Biocare Medical, Concord, CA, USA), and incubated with primary antibodies against rabbit $Na_v1.1$ (1:25; Alomone Labs) and GAD67 (1:100; Millipore). DyLight 488- and Cy3-conjugated secondary antibodies (1:200, Jackson ImmunoResearch Laboratories, West Grove, PA, USA) were used for signal detection. A total of six to eight brain sections (with 40 μm interval) per brain were analyzed. Images were examined using a confocal microscope (Carl Zeiss LSM 780, Oberkochen, Germany). Images were then analyzed using Axiovision software (Carl Zeiss) to quantify the amount of GAD67-positive (GAD67(+)), $Na_v1.1$-positive ($Na_v1.1$(+)), and $Na_v1.1$-expressing GAD67-positive ($Na_v1.1$-GAD67(+)) neurons in DG, CA3, and CA1. To quantify the immunohistochemical result, the intensity of 5 random 40 μm × 40 μm square areas from the background area were averaged as the baseline intensity. Positive staining signal was defined as the signal that had an intensity above 2.5 times of the baseline intensity, with staining area equal or larger than 80 μm^2, and was colocalized with the cells that were reactive to DAPI staining. All scoring was done in a blind fashion with respect to genotype and was performed by two independent investigators.

Preparation of hippocampal slices

Male mice at PW3 and PW4 were decapitated, and the brains were quickly removed and immersed in ice-cold oxygenated cutting solution consisting of (in mM): 250 sucrose, 2.5 KCl, 0.5 $CaCl_2$, 5 $MgCl_2$, 26 $NaHCO_3$, 1.26 NaH_2PO_4, and 15 glucose. The solution was aerated to a pH of ~7.4 with 95% O_2/ 5% CO_2. Coronal brain slices (350 μm) were cut in cutting solution using a vibratome (DTK-1000, Dosaka, Kyoto, Japan). The slices were then transferred to a holding chamber containing artificial cerebrospinal fluid (ACSF) consisting of (in mM): 125 NaCl, 2.5 KCl, 2 $CaCl_2$, 1 $MgCl_2$, 26 $NaHCO_3$, 1.26 NaH_2PO_4, 15 glucose, aerated with 95% O_2/5%CO_2. The slices were maintained at room temperature (23 ± 2 °C) for at least 1 hr before recording. For recording, the brain slices were placed in a recording chamber and continuously perfused with aerated ACSF. Whole-cell patch-clamp recordings were acquired at room temperatur (Molre with an Axopatch 200B amplifieecular Devices), using patch electrodes with resistance of 3 to 8 MΩ.

Electrophysiological recordings

The properties of $Na_v1.1$-expressing neurons were evaluated in PV(+) GABAergic neurons (Ogiwara et al., 2007) in *Gad1*$^{GFP/+}$:*Scn1a*$^{+/+}$ and *Gad1*$^{GFP/+}$:*Scn1a*$^{E1099X/+}$ mice at PW3 (5 *Gad1*$^{GFP/+}$:*Scn1a*$^{+/+}$ mice and 3 *Gad1*$^{GFP/+}$:*Scn1a*$^{E1099X/+}$ mice) and PW4 (6 *Gad1*$^{GFP/+}$:*Scn1a*$^{+/+}$ mice and 4 *Gad1*$^{GFP/+}$:*Scn1a*$^{E1099X/+}$ mice). *Gad1*^{GFP}-expressing neurons chosen for recording were fast-spiking basket cells with large soma, located at the border between the hilus and the granule cell layer of the DG (Liu et al., 2014; Martina et al., 1998). All of the recordings were performed at room temperature. The APs of GFP-expressing neurons were recorded under current clamp using a K-gluconate-based internal solution containing (in mM): 140 K-gluconate, 9 NaCl, 1 $MgCl_2$, 1 EDTA, 10 HEPES, 2 Mg-ATP, 0.3 Na-GTP, and 0.4% biocytin, pH 7.3 using KOH. A series of depolarizing currents was applied to patched neurons, and the features of the AP spike trains were analyzed offline. Input resistance was calculated from the voltage response between steady state and a 1-s hyperpolarizing current injection of −50 pA. The properties of a single AP were measured from the first AP elicited by the depolarizing protocol. The AP threshold was determined as the first point in the voltage trajectory with a slope change exceeding 20 V/s. The AP amplitude was measured from the threshold to the peak of the spike. Spike adaptation was quantified by the spike number reduction in the third 100 ms in relation to the spike number in the first 100 ms at 1000 pA current step ((spike number during 1st 100 ms) − (spike number during 3rd 100 ms)/(spike number during 1st 100 ms) × 100) (Butt et al., 2005). AP amplitude adaptation was assessed by the amplitude reduction of the last AP in relation to the amplitude of the initial AP at 1000 pA step ((amplitude$^{1st\ AP}$) − (amplitude$^{last\ AP}$) / (amplitude$^{1st\ AP}$) × 100). The slopes were calculated during the 10-90% rising phase and the 90-10% falling phase of the AP. The AP half-width was measured as the width at half-maximal amplitude. Afterhyperpolarization (AHP) was measured as the voltage difference between the threshold and the most negative voltage point after the AP.

Biocytin was infused into patched neurons during recording as a marker. After recording, slices containing biocytin-filled cells were fixed with 4% paraformaldehyde overnight at 4 °C. The slices were then incubated with Texas Red-avidin (1:200; Vector Labs, Burlingame,

CA, USA) and mouse anti-PV primary antibody (1:500; Millipore) followed by Cy5-conjugated anti-rabbit IgG (1:200; Jackson ImmunoResearch Laboratories). The data were analyzed only from PV-positive neurons.

To study postsynaptic properties of DG granule cells, hippocampal slices were prepared from WT and Het mice at PW4. The spontaneous postsynaptic currents (sPSCs) of granule cells were recorded in the presence of 3 mM kynurenic acid for spontaneous inhibitory postsynaptic currents (sIPSCs), or in the presence of 100 μM picrotoxin (PTX) for spontaneous excitatory postsynaptic currents (sEPSCs). The recording was done at a holding potential of −70 mV in a CsCl-based internal solution containing (in mM): 140 CsCl, 9 NaCl, 1 $MgCl_2$, 1 EDTA, 10 HEPES, 10 QX-314, 2 Mg-ATP, 0.3 Na-GTP, and 0.4% biocytin, pH 7.3 using CsOH. Miniature IPSCs (mIPSCs) and EPSCs (mEPSCs) were recorded under identical conditions with 1 μM tetrodotoxin (TTX; Tocris, Bristol, UK). To evaluate the paired-pulse ratio (PPR), pulses evoked by extracellular stimulation of the perforant pathway were delivered at 50-ms intervals, and the PPR was calculated by dividing the amplitude of the second EPSC by that of the first. The data were acquired using Clampex 10.2 software (Molecular Devices), filtered at 5 kHz, digitized at 10 kHz, and recorded using AxoScope 10.2 software (Molecular Devices). Access resistance was monitored at regular intervals throughout each experiment, and recordings were discarded if the values changed by > 20%. The AP firing activity was analyzed using Clampfit 10.2 (Molecular Devices). Miniature synaptic events were analyzed using Mini Analysis Program v6.0 (Synaptosoft, Fort Lee, NJ, USA). sIPSCs were examined in 7 WT and 6 Het mice, sEPSCs in 9 WT and 10 Het mice, mIPSCs in 3 WT and 4 Het mice, and mEPSCs in 7 WT and 9 Het mice.

Golgi staining

The Golgi-Cox method (Chen et al., 2012) was used to reveal the morphological features of DG granule cells. Brain samples were collected from WT and Het mice at PD14-PD16 (12 mice for each genotype) and PD21-PD24 (9 WT mice and 11 mice). The specimens were placed in impregnation solution from the FD Rapid GolgiStain kit (NeuroTechnologies, Ellicott City, MD, USA), and DG granule cells were imaged, reconstructed, and analyzed using the Stereo Investigator system (Microbrightfield Bioscience, Williston, VT, USA) and Neurolucida software (Microbrightfield Bioscience), as previously described (Chen et al., 2012). Dendritic segments were classified as branch segments (between two branching points) or terminal segments (between a branching point and terminal ending). The density of dendritic spines was measured in proximal segments (<50 μm from soma) and distal segments (>100 μm from soma) (6 mice for each age group).

Statistical analysis

The data were analyzed by GraphPad Prism 6 (GraphPad Software Inc, La Jolla, CA, USA). The results of Figs. 1f, 4c, 5a-d bottom insets, and f were analyzed using two-tailed unpaired Student's *t*-test. For Figs. 2a, i, 3d–f, 4d–e, g–k, and 6, the results were first analyzed by a two-way analysis of variance (ANOVA) with genotype as one of the variables. *Post-hoc* analysis (Bonferroni test) was performed when the ANOVA test yielded a significant main effect for genotype or a significant interaction between genotype and the second variable. The result of these two-way ANOVA tests was summarized in Supplement Table 1. In the case of spontaneous and miniature PSCs (Figs. 5a-d), PSCs from the same genotype were combined for the cumulative fraction and analyzed by Kolmogorov-Smirnov (K-S) test. For the frequency of spontaneous and miniature PSCs (Figs. 5a-d, bottom insets), the reported frequency was averaged from the mean frequency computed in each neuron based on genotype, and analyzed by unpaired *t*-test. All data are expressed as mean ± SEM. The asterisks indicate significant differences between groups: * $p < 0.05$; ** $p < 0.01$; *** $p < 0.001$.

Results

Generating a novel DS model: Scn1a^{E1099X} mice

We established a novel *Scn1a*-deficient mouse model based on the results from multiple clinical genetic screens (Depienne et al., 2009; Mancardi et al., 2006; Riva et al., 2009). A premature stop mutation (GAG → TAG) at amino acid residue E1099 (E1099X) of the *Scn1a* gene was introduced into the linker between domains 2 and 3 of $Na_v1.1$ (Fig. 1a). We then knocked the E1099X mutation into mouse ES cells (see recombination scheme in Fig. 1b). These ES cells were later used to derive chimeric mice (Figs. 1a–b). Heterozygous offspring from chimeric males and C57BL/6 females exhibited ~70% mortality in adulthood. Intercrosses of surviving heterozygous mice generated three genotypes at a typical Mendelian ratio (1:2:1). Genotyping by Southern blotting (Fig. 1d) and PCR (Fig. 1e) confirmed the expected genotypes of these offspring.

Similar to the strain-dependent mortality reported for several previous DS mouse models, the survival rate of Het mice varied depending on the strain background (Miller et al., 2014; Ogiwara et al., 2007; Yu et al., 2006). While most Het offspring in a pure 129 background developed normally and were fertile after puberty (premature death rate by PW4 = 5.4%, $n = 74$), 46.2% of Het in the C57BL/6 and 129 mixed backgrounds (~75%/25%) died by PW4. To characterize the pathology resulting from $Na_v1.1$ deficit, only mixed-background mice were used for further analysis. We next examined the expression of $Na_v1.1$ in the three *Scn1a^{E1099X}* allele genotypes using an N-terminal specific antibody against $Na_v1.1$. Global $Na_v1.1$ expression was reduced to 54.1% in Het mice and was undetectable in Homo mice compared to the controls (Fig. 1f). This result proved that our DS mouse model was a null mutation model and provided a preliminary molecular basis for the subsequent phenotype characterization.

Het mice recapitulated seizure susceptibility during early development.

During the first postnatal week, both Het and Homo pups were viable and without gross abnormalities. Beginning at PD9, Homo pups exhibited an unstable gait that deteriorated progressively. As early as PD12, Homo pups developed spontaneous generalized tonic-clonic seizures that lasted from 1 to 3 min (Movie 1). By PD15, these mice exhibited significantly lower body weight than WT or Het mice (Fig. 2a), likely due to malnutrition or dehydration. All of the Homo mice died by PD17 (Fig. 2b).

Het mice, on the other hand, developed seizure phenotype slightly later compared to the homozygous mice. In Het mice, spontaneous epileptiform activity began as early as PD20 (PW3) (Figs. 2c-d). Seizure activity in Het mice was closely followed in their home cages from PD20 to PD25 (Movie 2). To quantify seizure severity, seizures were scored from 1 to 5 based on Racine scale (Racine, 1972). During this period, 44.8% of animals exhibited spontaneous seizures (7 of 17 males and 6 of 12 females). Among these animals, a subset had undulating patterns of seizures, with the severity score surging or dropping abruptly during the episode. In the mice that died during the observation, the average number of episodes of spontaneous seizures was 5.8 ± 1.5, with some dying after a single episode (Fig. 2e). The average seizure duration was 45.8 ± 2.2 s (Fig. 2f), and the mean latency from first seizure onset to death was 13.9 ± 5.2 h (Fig. 2g). The animals that experienced severe seizure attacks (Racine scale stage 5) died at the average age of PD21.9 (Fig. 2h). Taken together, our results strongly suggest a close connection between *Scn1a* dysfunction and spontaneous seizure as well as sudden unexpected death (Sakauchi et al., 2011).

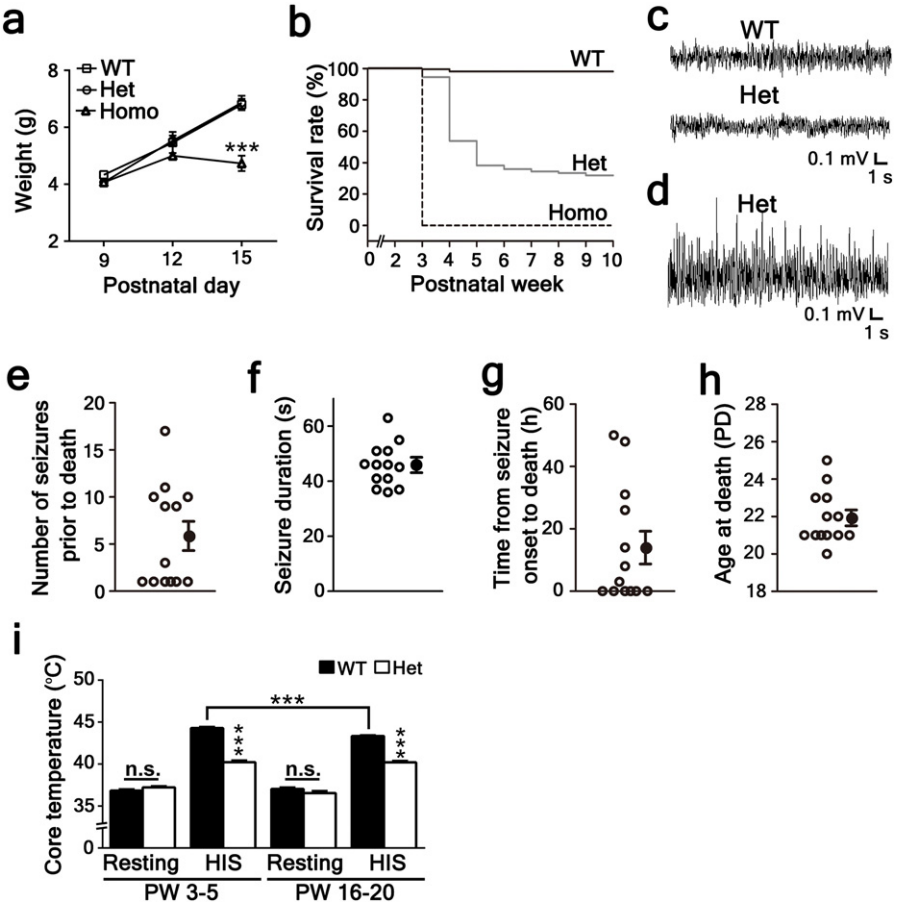

Fig. 2. Premature death, spontaneous seizures, and HISs in *Scn1a*^{E1099X} mice. a. Homo mice showed much less body weight compared to WT and Het mice ($ps < 0.001$ for group comparison at PD15, Bonferroni test). No significant difference was observed between WT and Het mice (3 mice for each genotype). b. The presence of *Scn1a*^{E1099X} allele reduced survival rate. WT = 100 mice; Het = 401 mice; Homo = 50 mice. c, d. Het mice exhibited obvious epileptic activity during spontaneous seizure. Representative EEGs from a WT and a Het mouse at PW10 during the interictal period without epilepsy (c) and a Het mouse during an ictal period with epileptic activity (d) (3 mice for each genotype). e–h. Characterization of spontaneous seizures in Het mice at PD20-PD25. Each open circle represents an individual animal; the closed circles denote the mean ± SEM ($n = 13$). Total amount of mice used for recording: 5 WT mice and 29 Het mice. i. Het mice showed a lower temperature threshold during HISs ($ps < 0.001$ for both age groups, Bonferroni test). The rectal temperature was measured at baseline and immediately following the onset of HISs (20 mice/age for each genotype; n.s., not significant).

DS infants are highly susceptible to epileptic attacks under hyperthermic conditions. To test if our *Scn1a*$^{E1099X/+}$ mice were also sensitive to HISs, we examined the HIS threshold at serial developmental time points. The threshold temperatures of HISs in WT and Het mice were compared at PW3-PW5 and PW16-PW20 (Fig. 2i). The threshold temperatures in Het mice at PW3-PW5 were significantly lower than those in WT mice regardless of sex (Het: 40.2 °C in males and 40.1 °C in females; WT: 44.3 °C in males and 44.7 °C in females; average temperature for both males and females are presented in Fig. 2i). The reduced threshold of HISs persisted into adulthood (PW16-PW20; Het: 40.2 °C in males and 40.0 °C in females; WT: 43.3 °C in males and 43.6 °C in females; average temperature for males and females are presented in Fig. 2i). Thus, the major phenotypes of Het mice, including premature death, spontaneous seizures, and increased susceptibility to HISs, remarkably resembled the key features observed in DS patients. As we observed a developmental transition between PW3 and PW4, during which the emerging spontaneous seizures were accompanied with surging mortality, we focused on developmental abnormalities of $Na_v1.1$ expression and epileptogenic network dysfunction primarily within this time window.

Preferential reduction of $Na_v1.1$-expressing interneurons in hippocampal DG

The hippocampus is a major epileptogenic zone (de Lanerolle et al., 1989; Lothman et al., 1992). Studies in other *Scn1a* mutant models have suggested that the hippocampus contributes to epilepsy initiation in HISs (Liautard et al., 2013; Ohno et al., 2011). We therefore focused on the hippocampus to examine how the genetic deficit in *Scn1a* affected the temporal expression of $Na_v1.1$ during early development, when frequent spontaneous seizures emerged. $Na_v1.1$ protein levels in the hippocampus were quantified in WT and Het mice at PW3, PW4, and PW6 (Fig. 3a). Hippocampal $Na_v1.1$ expression in male WT mice was dramatically increased from PW3 to PW4 and became stable thereafter (Fig. 3b). In Het mice, however, the overall $Na_v1.1$ level across ages was less than 50% of that in WT (Fig. 3b). A similar reduction of $Na_v1.1$ was seen in female Het mice (Fig. S1). Because we did not observe a detectable difference of $Na_v1.1$ expression between male and female animals, we focused on male animals in the following studies.

$Na_v1.1$ is primarily expressed in GABAergic neurons in the hippocampus (Ogiwara et al., 2007; Yu et al., 2006). We next quantified the proportion of $Na_v1.1$-expressing GAD67-positive neurons ($Na_v1.1$-GAD67(+)) in the hippocampus (Fig. 3c). In WT mice, ~80% of GAD67(+) neurons expressed $Na_v1.1$ across the DG, CA3, and CA1 at both PW3 and PW4. Despite having similar amount of GAD67(+) neurons, the percentage of Nav1.1-GAD67(+) neurons in DG was significantly reduced to 58% at PW3 and further decreased to 39.2% at PW4 (Figs. 3e-f). Unlike DG, both CA3 and CA1 exhibited relatively normal levels of $Na_v1.1$-GAD67(+) cells until PW4, at which point the percentage of $Na_v1.1$-expressing cells decreased to about 60% (61% for CA3 and 62.4% for CA1) (Figs. 3e–f). A reduction of $Na_v1.1$-GAD67(+) neurons, particularly in the DG, coincided with overall lower

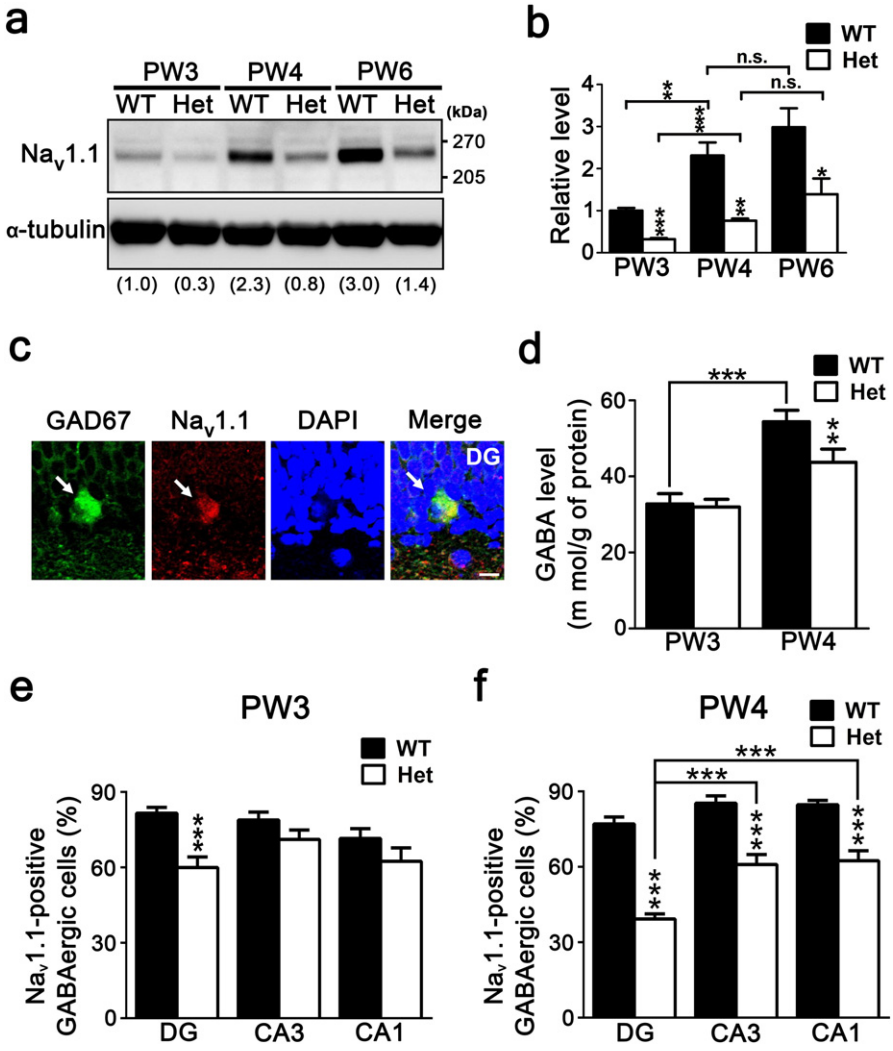

Fig. 3. Hippocampal $Na_v1.1$ expression was compromised in Het mice. a, b. Het mice showed reduced hippocampal $Na_v1.1$. Immunoblots were performed with total hippocampal lysates from PW3, PW4, and PW6 mice (5 mice for each age group). The expression level was normalized to α-tubulin before being normalized to that of WT mice at PW3 (set as 1 in b). c. $Na_v1.1$ (red) colocalized with GAD67 (green)-expressing neurons in DG from PW4 animals. Scale bar, 10 μm. d. GABA level was significantly reduced in Het compared to WT at PW4 ($p < 0.01$ at PW4, Bonferroni test). The GABA content was measured by ELISA (4 mice for PW3 and 11 for PW4 for each genotype). e, f. The percentage of $Na_v1.1$-GAD67(+) neurons in Het mice were preferentially reduced in the DG at PW3 (Het: 58%, WT: 81.6%) and further reduced at PW4 (Het:39.2%, WT: 77%) compared to CA3 and CA1 (CA3: Het: 70.9% and WT: 78.8% at PW3; Het: 61% and WT: 85.3% at PW4; CA1: Het: 63.4% and WT: 71.5% at PW3; Het: 62.4% and WT: 84.7% at PW4). At PW3, a significant reduction of the percentage of $Na_v1.1$-GAD67(+) neurons in Het hippocampus was present only in the DG region ($p < 0.001$, Bonferroni test). At PW4, the significant reduction was present in all 3 regions in Het compared to WT mice ($ps < 0.001$, Bonferroni test). A step-down ANOVA showed a significantly lower percentage of DG $Na_v1.1$-GAD67(+) neurons compared to CA3 and CA1 ($F(2, 62) = 15.3$, $p < 0.001$, one-way ANOVA; $ps < 0.0001$, Bonferroni test) (3 mice for each age group).

hippocampal GABA levels at PW4 (Fig. 3d). Taken together, we found that the Het hippocampus suffered a severe reduction of $Na_v1.1$ expression during development, with the majority of $Na_v1.1$-GAD67(+) neurons lost in the DG. These results provided cytological evidence of a progressively abnormal hippocampal network, with the most severe effect in the DG. It was also noted that this effect coincided with surging spontaneous seizures in Het mice.

Het DG GABAergic neurons were incapable of high-fidelity firing

The DG GABAergic circuit plays a significant role in gating major excitatory input into the hippocampus. Based on the greatest degree of reduction of $Na_v1.1$ expression in the DG, we next examined AP firing properties in DG interneurons in acute hippocampal slices at PW3 and PW4. We particularly focused on PV(+) interneurons, as the majority of PV(+) interneurons express $Na_v1.1$ (Dutton et al., 2012; Ogiwara et al., 2007). DG GABAergic neurons were identified by Gad-driven GFP in $Gad1^{GFP/+}$:$Scn1a^{+/+}$ and $Gad1^{GFP/+}$:$Scn1a^{E1099X/+}$ mice. During recording, biocytin was infused into the patched neurons, and a *post hoc* immunohistochemistry was performed to confirm PV expression in the recorded neurons (Fig. 4a). Morphological reconstruction showed that our recorded neurons had characteristic features of fast-spiking PV(+) DG interneurons, with the majority of their axons densely distributed within the granule layer (Fig. 4b) (Liu et al., 2014). The morphology of these neurons also resembled a subclass of DG basket cells, which form perisomatic synapses on DG granule cells (Jonas et al., 2004).

To examine the excitability of DG GABAergic neurons, APs were elicited by a series of step current injections (Fig. 4c). While there was no significant difference in input resistance compared to the control neurons, $Gad1^{GFP/+}$:$Scn1a^{E1099X/+}$ PV(+) neurons showed drastically lower excitability across various levels of current injection (Figs. 4c-e). In addition to low excitability, $Gad1^{GFP/+}$:$Scn1a^{E1099X/+}$ neurons exhibited unusual spike adaptation. Control fast-spiking PV(+) neurons normally had very little or no adaptation during suprathreshold depolarization. In contrast, $Gad1^{GFP/+}$:$Scn1a^{E1099X/+}$ neurons showed a profound adaptation in firing (spike number reduction: 29.98 ± 3% in control and 78.9 ± 15.4% in $Gad1^{GFP/+}$:$Scn1a^{E1099X/+}$ neurons at 1000 pA injection)

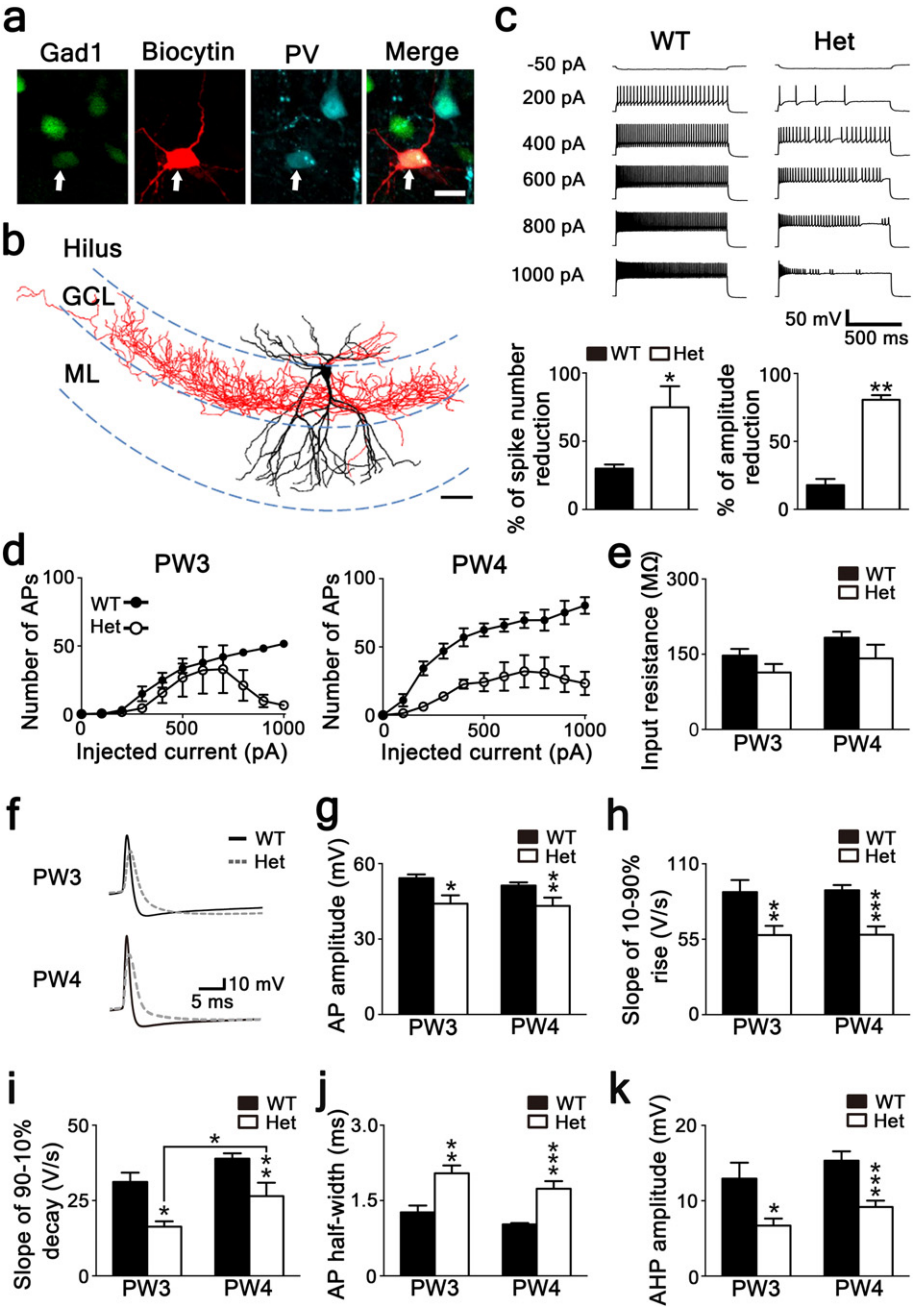

Fig. 4. The electrophysiological characteristics of DG PV(+) interneurons were significantly altered in Het mice. a. An example of a recorded neuron from a *Gad1*$^{GFP/+}$:*Scn1a*$^{+/+}$ mouse (green). Biocytin (red) was infused to mark the patched neuron during recording. The expression of PV was confirmed by post hoc immunohistochemistry (blue). Scale bar, 20 μm. b. Morphological identification of a recorded neuron. The axon of the recorded cell is shown in red; the soma and dendrites are indicated in black. GCL, granule cell layer; ML, molecular layer. Scale bar, 50 μm. c. DG PV(+) interneurons from *Gad1*$^{GFP/+}$:*Scn1a*$^{E1099X/+}$ mice showed reduced excitability and apparent spike adaptation. Top, examples of AP traces recorded from PV(+) interneurons at PW4. Bottom, percentage reduction of spike number (left) and amplitude (right) in response to 1000 pA injection. d. Input–output relation of evoked spike numbers in response to a series of current injections showed reduced excitability in PV(+) neurons from *Gad1*$^{GFP/+}$:*Scn1a*$^{E1099X/+}$ mice. The lower excitability of Het neurons was particularly significant when the injected current was higher than 800 pA at PW3 ($ps < 0.01$ for 900 pA and above, Bonferroni test). At PW4, low excitability was significant when the injected current was higher than 100 pA ($ps < 0.01$ for 200 pA and above, Bonferroni test). e. No significant difference in input resistance between *Gad1*$^{GFP/+}$:*Scn1a*$^{E1099X/+}$ PV(+) neurons and *Gad1*$^{GFP/+}$:*Scn1a*$^{+/+}$ neurons. f. Examples of a single AP trace from WT (black) and Het (dash gray) neurons. g–k. *Gad1*$^{GFP/+}$:*Scn1a*$^{E1099X/+}$ PV(+) neurons showed altered AP features. g. AP amplitude was reduced in Het ($ps < 0.05$ for both age groups, Bonferroni test). h. AP from Het neurons exhibited a much slower rise phase ($ps < 0.01$ for both age groups, Bonferroni test). i. AP from Het neurons showed a slower decay phase ($ps < 0.05$ for both age groups, Bonferroni test). j. AP from Het neurons exhibited wider half-width ($ps < 0.01$ for both age groups, Bonferroni test). k. AP from Het neurons showed smaller AHP amplitude ($ps < 0.05$ for both age groups, Bonferroni test). PW3: 5 neurons from 5 *Gad1*$^{GFP/+}$:*Scn1a*$^{+/+}$ mice and 3 neurons from 3 *Gad1*$^{GFP/+}$:*Scn1a*$^{E1099X/+}$ mice. PW4: 6 neurons from 6 *Gad1*$^{GFP/+}$:*Scn1a*$^{+/+}$ mice and 4 neurons from 4 *Gad1*$^{GFP/+}$:*Scn1a*$^{E1099X/+}$ mice.

and in AP aptitude at higher frequencies (amplitude reduction: 12.77 ± 4.59% in control and 80.60 ± 3.41% in *Gad1*$^{GFP/+}$:*Scn1a*$^{E1099X/+}$ neurons at 1000 pA injection) (Fig. 4c bottom). Moreover, *Gad1*$^{GFP/+}$:*Scn1a*-$^{E1099X/+}$ neurons showed frequent failure in firing, with apparent missing spikes during high frequency activity (Fig. 4c). Despite low excitability, *Gad1*$^{GFP/+}$:*Scn1a*$^{E1099X/+}$ neurons, to our surprise, exhibited a slightly more depolarized resting membrane potential compared to the control neurons (Fig. S2).

Further AP waveform analysis revealed altered AP features in *Scn1a*-deficient neurons. Compared to the control neurons, *Gad1*$^{GFP/+}$:*Scn1a*-$^{E1099X/+}$ neurons had much lower AP amplitudes (Figs. 4f, g). In addition, AP in *Scn1a*-deficient neurons showed a much slower time course in

both depolarization and repolarization phases, which resulted in broadened APs (Figs. 4f, h–j). Such slow depolarization was followed by abnormal hyperpolarization patterns, with fast AHP amplitude being significantly reduced (Figs. 4f, k).

A compensatory up-regulation of $Na_v1.3$ expression has been shown in hippocampal GABAergic neurons in a *Scn1a*$^{+/-}$ DS mouse model (Yu et al., 2006). Compensatory changes in the expression of ion channels might offer some explanation for the AP abnormality. We therefore examined the expression of the α subunits of other sodium channels ($Na_v1.2$, $Na_v1.3$, and $Na_v1.6$) and a fast spiking-required potassium channel ($K_v3.2$) in Het mice. Contrary to the previous report, we found no detectable change in the expression of these sodium and potassium channels in Het animals (Fig. S3). We also examined the levels of these ion channels in Homo animals. We found that $Na_v1.6$, a genetic modifier of $Na_v1.1$ mutations, was downregulated (Fig. S3c), whereas $K_v3.2$ was upregulated in Homo mice (Fig. S3d).

Taken together, our results revealed the severe impact of sodium channel-insufficiency on the electrophysiological abnormality in Het PV(+) interneurons. Such aberrant excitability of PV(+) interneurons would greatly compromise the strength and precision of inhibitory control in the DG network.

Scn1a insufficiency selectively elevated basal excitatory transmission in DG

To delineate the impact of deficient GABAergic input on network transmission, we examined the spontaneous IPSCs and EPSCs received at DG granule cells, the major DG principal neurons, in acute hippocampal slices. In order to avoid within-network bias on assessing excitatory versus inhibitory transmission, we sampled IPSCs and EPSCs from independent animals for each genotype, with minimal amount of neurons sampled in each animal (Fig. 5 legend). In Het granule cells, the frequency of sIPSCs was significantly reduced, whereas sEPSC frequency was increased compared with control cells (Figs. 5a–b). Despite the change in frequency, the amplitudes of sIPSCs and sEPSCs from Het neurons were indistinguishable from those of control neurons (Figs. S4a–b). These results indicated the changes of neurotransmission following $Na_v1.1$ deficiency occurred in the presynaptic terminals. To understand whether the change of

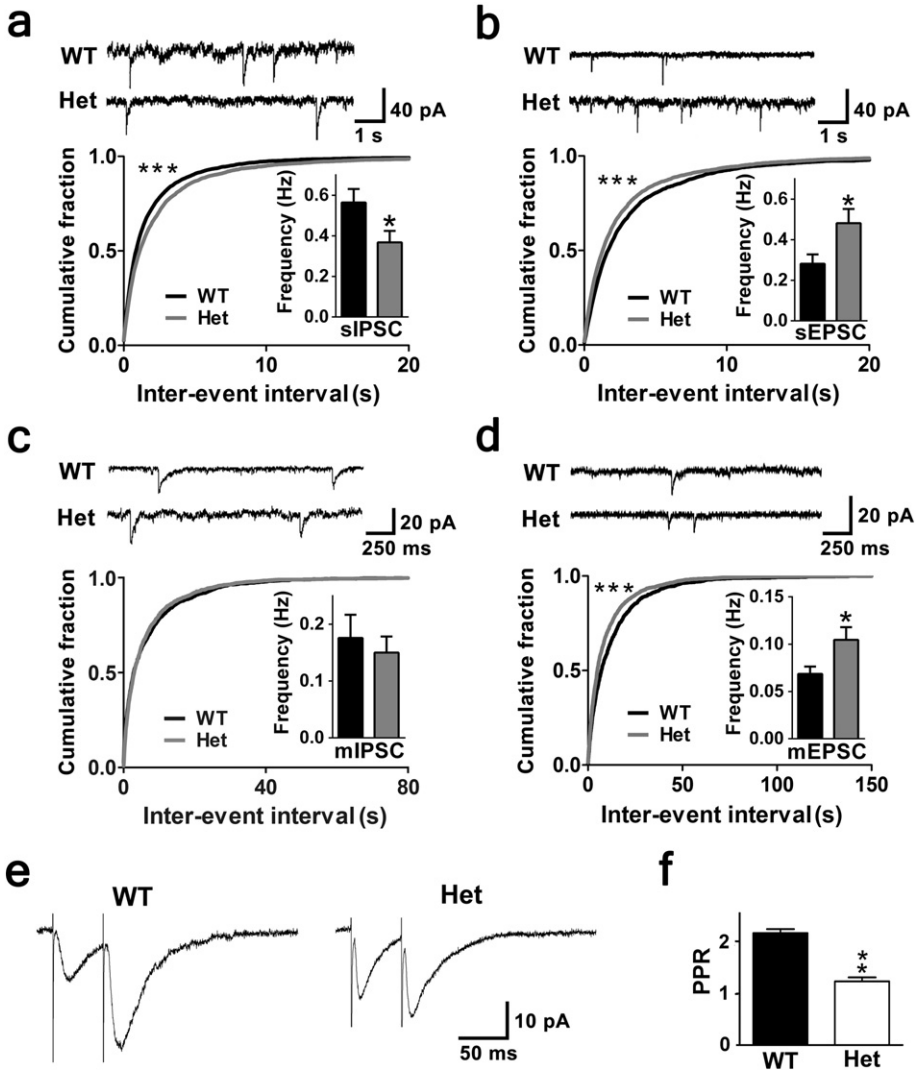

Fig. 5. The DG network exhibited imbalanced activity in Het mice. a, b. Recordings in DG granule cells showed a decreased frequency of sIPSCs (a) and an increased frequency of sEPSCs (b). Top: sample traces of sPSC recordings over a 10-second span. Bottom: cumulative plots of sPSCs. Bottom inset: average frequency of sPSCs (a and b: *p*s < 0.001 for cumulative fraction, K-S test. $p < 0.05$ for averaged frequency, unpaired *t*-test) (sIPSC: 16 neurons from 7 WT mice and 20 neurons from 6 Het mice. sEPSC: 21 neurons from 9 WT mice and 20 neurons from 10 Het mice). c. mPSC recordings revealed no change in mIPSC frequency ($p = 0.101$ for cumulative fraction, K-S test. $p = 0.6$ for averaged frequency, unpaired *t*-test) (7 neurons from 5 WT mice and 5 neurons from 4 Het mice). d. An increased mEPSC frequency was observed in Het neurons ($p < 0.001$ for cumulative fraction, K-S test. $p < 0.05$ for frequency, unpaired *t*-test) (18 neurons from 7 WT mice and 14 neurons from 9 Het mice). Top: sample traces of mPSC recording. Bottom: cumulative plots of mPSCs. Bottom inset: average mPSC frequency. e, f. Paired pulse stimulation showed increased release probability of excitatory terminals in Het mice. e. Sample traces of EPSCs evoked in DG granule cells by paired stimuli at 50-ms intervals. f. A reduced paired-pulse ratio (PPR, 2nd EPSC/1st EPSC) was evident in neurons from Het mice (4 neurons from 2 mice for each genotype).

sPSC frequency was associated with an altered machinery of presynaptic transmitter release, we examined miniature PSCs in DG granule cells in the presence of the sodium channel blocker TTX (Figs. 5c–d). In the Het neurons, the frequency and amplitude of mIPSCs were indistinguishable from the controls (Fig. 5c). In contrast, mEPSCs showed a much higher frequency (Fig. 5d). Despite the increase in frequency, mEPSC amplitude was similar to the control (Figs. S4c–d). Increased mEPSC frequency likely suggested a heightened presynaptic release probability. To further examine the release probability of excitatory terminals, we measured the synaptic response of brief paired stimuli with 50-ms intervals. The paired-pulse ratio (PPR, EPSC2/EPSC1) in Het mice was significantly lower than that in the controls (Figs. 5e–f). This result strongly supported the idea that the release probability of excitatory terminals was elevated in Het granule cells (Zucker, 1989).

Taken together, our results revealed imbalanced excitatory and inhibitory inputs to DG granule cells as a result of weakened GABAergic input within the network. Most importantly, the release probability of excitatory terminals was significantly elevated in granule cells in this network. This increased excitatory release probability could further exacerbate the already hyperexcitable network by promoting runaway excitation. Additionally, the imbalanced network activity likely has a strong impact on the morphological development of DG neurons, as the fine-tuning of neuronal connection is highly activity-dependent.

Scn1a-deficient DG granule cells exhibited progressively altered dendritic profile

Developmental remodeling of dendrites and synapses is partly activity-dependent (Wong and Ghosh, 2002). The chronic imbalance of excitatory and inhibitory inputs to DG granule cells would potentially affect its dendritic and spine restructuring. To examine if imbalanced network activity alters the structural remodeling of DG neurons, we reconstructed dendritic profiles of Golgi-impregnated granule cells (Fig. 6a). In the initial analysis that examined bifurcation numbers and the amount of terminal endings of dendrite branches, Het granule cells did not appear to be much different from the control cells (Figs. 6a-c). Further analysis, however, revealed that development-dependent dendritic arborization in Het granule cells was greatly altered at PW4. The alteration manifested as a reduction in the number of dendritic segments and the total dendritic length (Figs. 6d, f). It should be noted that the decrease of dendritic length was due to a lower overall number of dendritic segments but not a shorter average segment length (Figs. 6d–f), suggesting a reduced dendritic complexity. We also observed a slightly longer segment length in Het neurons in PW3, but this difference was absent by PW4 (Fig. 6e). To further verify the reduced dendritic complexity during development, we applied Sholl analysis (Chen et al., 2012; Sholl, 1953), which measures the number of intersections between dendrites and superimposed concentric circles centered on the centroid of the soma (Fig. 6g). This analysis revealed a greater reduction in dendritic complexity in Het neurons, especially in the distal region (>100 μm from the soma) at PW4 (Figs. 6h-i). In addition to dendritic features, we examined the developmental change of spine density. In the control neurons, normal pruning during PW3 and PW4 resulted in a significant reduction of spine density at both proximal (<50 μm from the soma) and distal (>100 μm from the soma) segments (Figs. 6j-k). In contrast, dendritic spines in Het neurons did not undergo such normal pruning, leaving spine density unchanged across both developmental stages (Fig. 6k).

Taken together, our results uncovered a progressively altered dendritic architecture in Het granule cells. Abnormal dendritic arborization likely hinders proper signal integration in the DG cells and contributes to the cognitive deficits seen in DS mice and patients. More importantly, excess spines could result in greater excitatory input to the granules cells, which, in combination with heightened excitatory neurotransmission probability and dampened inhibitory control, could easily result in runaway excitation in the DG network.

Discussion

In this study, we demonstrate that epileptic channelopathy in a DS model with *Scn1a* mutation causes pro-epileptic network activity in the DG by directly reducing inhibitory input as well as elevating excitatory input through functional adaptation during development. This developmental network deficit coincides with progressive worsening of spontaneous seizures and premature mortality. These results are largely in agreement with the conclusion from previous works that focus on different brain areas (Cheah et al., 2012; Han et al., 2012; Ogiwara et al., 2007; Yu et al., 2006). In addition to functional assessment, we examined structural changes of DG granule cells in *Scn1a*-deficient mice. Our result unveils previously undescribed age-dependent morphological alterations (reduced distal dendritic complexity with excess proximal spines) of DG granule neurons in *Scn1a*-deficient animals. Because these morphological alterations likely further increases network vulnerability to epileptic activity and could have a long term impact on higher-order cognitive processing, our overall finding points to the urgency of clinical intervention during early development.

General phenotype of spontaneous seizures and HISs in E1099X/+ models

Our results demonstrate that the Het mouse model exhibits phenotypes that are reminiscent of DS patients. These phenotypes, which include spontaneous seizures, HISs and seizure-induced mortality in early development, also match the phenotypes seen in other DS mouse models (Cheah et al., 2012; Ogiwara et al., 2007; Yu et al., 2006). It has been reported that the seizure severity of heterozygous *Scn1a* alleles varies by strain background (Mistry et al., 2014). We observed a similar strain-dependent impact on the phenotype of the $Scn1a^{E1099X}$ allele. In the 129 strain background, Het animals developed normally. In contrast, Het in a mixed B6:129 background gave rise to a seizure phenotype that is comparable to other DS mouse models (Miller et al., 2014; Ogiwara et al., 2007; Yu et al., 2006). It is worth noting that, in the same B6:129 N2 background, Het mice exhibited higher lethality compared to other heterozygous *Scn1a* null alleles (at PW4: Het mice: 40%, $Scn1a^{RX/+}$ mice: 20%, $Scn1a^{tm1Kea/+}$ mice: 30%) (Miller et al., 2014; Ogiwara et al., 2007). This difference points to the significant role of predisposing genetic components as well as the nature of *Scn1a* mutation with respect to seizure severity. In the case of genetic composition influence, several Dravet survival modifier loci have been identified in mouse (Miller et al., 2014). In addition, candidate modifiers show strain-dependent expression. These modifiers include GABA-A receptor subunits (*Gabra2, Gabra6, Gabrb2*, and *Gabrg3*), voltage-dependent calcium channel subunits (*Cacna1a* and *Cacna2d1*), potassium channel (*Kcnj11*), and chloride channel (*Clcn3*) (Miller et al., 2014). The combination of such genetic variations would have a major impact on neuronal excitability and seizure susceptibility (Bian et al., 2006; Burgess and Noebels, 2000; Dickerson et al., 2002; Gloyn et al., 2006; Hernandez et al., 2011; Macdonald et al., 2012; Yamada et al., 2001). Further study of the physiological significance of these modifier genes in relation to *Scn1a* will provide greater insight into personalized treatment in DS patients.

Similar to DS patients and other DS models, Het mice exhibited a much lower threshold of HISs (Cao et al., 2012; Cheah et al., 2012). The detailed mechanism underlying HISs is unclear. One possibility is that a higher physical temperature may alter neural excitability by altering ion channel properties, and/or by preferentially affecting inhibitory neurotransmission (Brauchi et al., 2006; Carpenter and Alving, 1968; Gorman and Marmor, 1970). Indeed, slice recording at higher temperatures reveals elevated excitability in hippocampus as the result of either changes in ion equilibrium or changes in the pre- or postsynaptic properties of inhibitory neurons in the CA1 region (Qu and Leung, 2008;

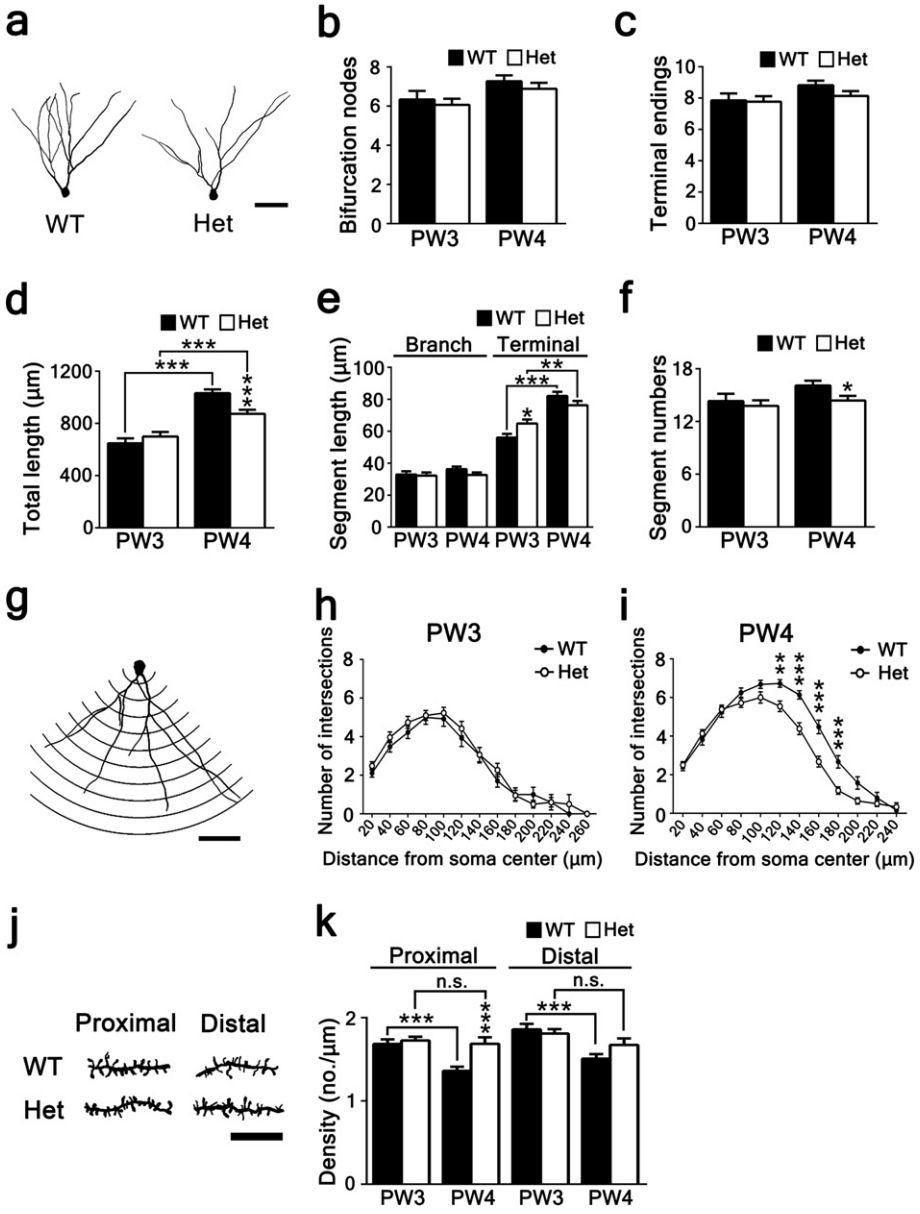

Fig. 6. The dendritic morphology of DG granule cells was altered in Het mice. a. Examples of reconstructed Golgi-stained DG granule cells. Scale bar, 50 μm. b—f. Quantitative comparison of the dendritic parameters in DG granule cells from mice at PW3 and PW4: number of bifurcation nodes (b), number of terminal endings (c), total length (d), segment length (e), and segment number (f). b, c. Het neurons showed no difference in the amount of bifurcation nodes and terminal endings. d. Total dendritic length was reduced in Het neurons at PW4 ($p < 0.001$ at PW4, Bonferroni test). e. No detectable difference of segment length between genotypes during development. Note that we observed a small increase of terminal segment length in PW3 Het neurons compared to WT neurons ($p < 0.05$, Bonferroni test). f. Segment number was reduced in Het neurons at PW4 ($p < 0.05$, Bonferroni test). g. A camera lucida drawing of a DG granule cell used for Sholl analysis. The number of dendritic intersections within each sphere was plotted against the radius from the soma. Scale bar: 50 μm. h, i. Dendritic complexity was reduced in Het DG granule cells at PW4, particularly in the distal regions (120–180 μm from soma) (*ps* < 0.01, Bonferroni test). For the sample size of Figs. 6b—i, PW3: 28 neurons from 12 WT mice and 31 neurons from 12 Het mice. PW4: 43 neurons from 9 WT and 43 neurons from 11 Het mice. j. Examples of Golgi-stained dendritic spines in the proximal and distal dendrites of DG granule cells. Scale bar: 10 μm. k. Abnormal spine pruning in Het mice. The difference in spine density between genotypes was particularly significant in the proximal region at PW4 ($p < 0.001$, Bonferroni test) (20 dendrites per 12 neurons from 6 mice for each age group).

Qu et al., 2007; Wu and Fisher, 2000). If this is true, raising the temperature of Het mice would certainly exacerbate the already seizure-prone DG network and further promote epileptic activity. Alternatively, HISs might result from hyperthermia-induced respiratory alkalosis (Schuchmann et al., 2006). For this reason, HISs in immature rats can be immediately reversed by supplying 5% CO_2 for inhalation (Schuchmann et al., 2006). Under normal conditions, HISs from paraventricular nuclear activation are not easily triggered due to strong local inhibition (Lovick and Coote, 1988). It is likely that such local inhibition is compromised due to preferential loss of functional $Na_v1.1$ in inhibitory neurons in *Scn1a* mutants. This hypothesis is supported by the observation that HISs can be immediately reverted by supplying 10% CO_2 for inhalation in other *Scn1a* mutants (Ohmori et al., 2013).

Impact of $Na_v1.1$ deficiency on neural network activity and development

Similar to other DS models, Het mice exhibited reduced $Na_v1.1$ expression across development. We observed a preferential reduction of $Na_v1.1$-expressing GABAergic neurons in DG compared to CA3 and CA1. This local-network specific reduction of $Na_v1.1$-expressing GABAergic neurons has also been reported in one DS model in which the mutant *Scn1a* is introduced specifically in GABAergic neurons

(Cheah et al., 2012). Therefore, network-specific alteration of $Na_v1.1$ expression in GABAergic neurons reflects a high heterogeneity of GABAergic neurons across networks and may help explain the epileptogenic nature of DG. Because $Na_v1.1$ is mainly expressed in the soma and the AIS, often being concentrated at nodes of Ranvier, $Na_v1.1$ deficits would certainly alter neuronal electrophysiological properties (Duflocq et al., 2008). We found that the resting membrane potential was more depolarized in Het hippocampal PV(+) interneurons compared to the control neurons. As we did not examine the features of the Na^+ current or other related currents in detail in these neurons, it is difficult to determine the underlying cause. Contrary to our observation, an elevated resting potential is not reported in other DS models (Ogiwara et al., 2007; Tai et al., 2014). This discrepancy might result from cell type-specific (in combination with strain differences) adaptation of the resting potential in response to sodium channel deficiency (Waxman, 2007).

In addition to an elevated resting potential, the firing properties of Het neurons were greatly compromised. The time course of the AP in Het PV(+) interneurons revealed overall slower AP dynamics with smaller AP amplitudes. Because *Scn1a*^{E1099X} is a null allele, these altered AP features are likely caused by lower and/or slower sodium influx as the result of the haploinsufficiency. This idea is supported by the observation that various mutations (nonsense and deletion) in *Scn1a* result in reduced Na^+ current in inhibitory neurons (Mistry et al., 2014; Ogiwara et al., 2007; Tai et al., 2014; Yu et al., 2006). In addition, because $Na_v1.1$ contains an important domain for local protein organization (Leterrier et al., 2011), $Na_v1.1$ insufficiency might affect the organization of other ion channels and/or regulatory proteins within AIS, resulting in aberrant sodium influx (Garrido et al., 2003; Lorincz and Nusser, 2008). Altered sodium dynamics will further reduce or retard the subsequent activation of potassium channels in the repolarization phase, leading to slower repolarization, wider APs, and smaller fast AHP (Bean, 2009; Jonas et al., 2004; Martina et al., 1998). The lower AHP reflects inadequate potassium channel activation, which may result from a reduced activation level of potassium channels due to the significantly lower sodium shooting. Alternatively, the smaller AHP might be caused by a decreased expression of potassium channels. Chronic low excitability, which leads to aberrant cellular signal transduction, likely hinder the activity and/or development-dependent expression of other ion channels and/or regulatory proteins. Changes in the expression of other sodium channels have been reported in another DS model (Yu et al., 2006) and rats with kainate-induced epilepsy (Qiao et al., 2013). When we examined the expression levels of these other ion channels, we found no detectable differences in the levels of global $Na_v1.2$, $Na_v1.3$, $Na_v1.6$, and $K_v3.2$ in our Het animals. Changes in channel expression were only seen in Homo animals, in which $Na_v1.6$ expression was decreased and $K_v3.2$ was increased. Differences in ion channel expression among DS models might reflect much more complex genetic mechanisms (e.g., strain differences, neuron and/or age-specific regulation) underlying the compensatory effect. A further systematic examination at the cell and/or circuit-specific level would offer more insight into the complex interplay among ion channel expression in DS models.

Abnormal APs are suggestive of the firing deficits of Het PV(+) neurons. These neurons were not merely less excitable but also were incapable of persistent firing at higher frequencies. The firing of these neurons also displayed abnormal spike adaptation with respect to both amplitude and frequency. Because the DG network relies heavily on the high fidelity of fast-spiking inhibition to set the baseline activity within the network, imbalanced network activity as the result of reducing inhibitory input is expected. Our results showed decreased sIPSC and increased sEPSC frequency in the DG, which is similar to the imbalanced network activity seen in CA1 in another DS model (Han et al., 2012). Despite differential changes in frequency, the sPSCs amplitudes in the present DS model were indistinguishable from those of controls, suggesting an unchanged postsynaptic function at both inhibitory and excitatory terminals. In contrast to our results, differential changes in sPSC amplitude in CA1 have been reported (Gu et al., 2014). Inherent network and strain differences as well as various subcellular impacts of *Scn1a* mutations likely contribute to the discrepancy. In contrast to unchanged postsynaptic properties, we observed elevated release probability at DG excitatory terminals, as evidenced by heightened mEPSC frequency and decreased PPR (i.e., decreased paired-pulse facilitation) in Het granule cells. Because granule cells receive excitatory inputs from local mossy cells and entorhinal afferents, the heightened excitatory release probability likely results from DG-autonomous hyperexcitability and/or enhanced extrinsic input (Amaral et al., 2007; Deller et al., 1996). Regardless of the source of these excitatory synapses, this observation points to a surprising pro-epileptic mechanism in addition to reduced network inhibitory control, namely, increased excitatory release probability might further exacerbate the already hyperexcitable DG network. In contrast to our result, no increase in mEPSC frequency in CA1 or the prefrontal cortex is observed in another DS model (Han et al., 2012). This difference may reflect a unique plasticity feature of excitatory terminals in DG granule cells and further supports the idea that the DG is especially vulnerable to epileptogenic activity.

The central neural networks make excessive connections in the early development. These connections are later strengthened, weakened, or eliminated based on their inherent genetic program and activity history (Tessier and Broadie, 2009). By examining dendritic morphology of DG granule cells during the developmental transition of emerging spontaneous seizures, we found that $Na_v1.1$ deficiency significantly dampened normal spine pruning, leading to excess proximal spines in Het granule cells at PW4. Excess proximal spines, in combination with elevated excitatory release probability, could facilitate runaway excitation, particularly when considering that PV(+) interneurons represent approximately 40% of DG basket cells (Ribak, 1992). PV(+) basket cells provide perisomatic inhibition to granule cells and receive extensive input from granule cells, thereby being linked to granule cells in a powerful feedback inhibition circuit in the DG (Ribak, 1992). Tipping the activity balance in granule cells by removing inhibitory control and elevating excitatory input both structurally and functionally (i.e., excess spines and heightened excitatory transmission and release probability) would undoubtedly lead to catastrophic epileptic activity in the network. In addition to abnormal spine pruning, we found that the complexity of distal dendrites was severely reduced. Distal dendritic structure in granule cells is specifically important for proper input integration as synaptic current at distal dendrites of granule cells has a very fast time course, resulting in a very narrow time window for temporal integration of synaptic inputs (Schmidt-Hieber et al., 2007). Reduced dendritic arborization could therefore decrease the accuracy and fidelity of signal propagation across the network, likely contributing to the cognitive deficits seen in other DS models (Han et al., 2012; Ito et al., 2013).

In conclusion, our results reveal plausible neural mechanisms underlying the developmental deficits of a novel DS model. Our results, showing the similar temporal profile between seizure onset and the underlying neural developmental abnormalities, could provide a useful clinical reference for medical intervention in DS patients during early development. In addition, the null mutation of the *Scn1a*^{E1099X} allele, known to cause DS in human patients, could serve as a powerful preclinical tool for treatment development.

Funding

Funding for this study was provided by National Taiwan University (103R7152), the Ministry of Science and Technology (MOST 103-2321-B-002-018), and the Ministry of Health and Welfare in Taiwan (MOHW103-TDU-PB-211-133008) for SW Lin, and the MEXT of Japan and Takeda Science Foundation for Y Yanagawa.

Supplementary data to this article can be found online at http://dx.doi.org/10.1016/j.nbd.2015.02.010.

Acknowledgments

We are grateful for the technical services provided by the Transgenic Mouse Model Core Facility of the National Core Facility Program for Biotechnology, Ministry of Science and Technology, Taiwan, and the Gene Knockout Mouse Core Laboratory of National Taiwan University Center of Genomic Medicine, and the Cell Imaging Core of the First Core Labs in the National Taiwan University Center of Medicine. We thank Dr. Ming-Yuan Min for providing the *Gad1*$^{GFP/+}$ mice in house as well as Dr. Cheng-Chang Lien and Dr. Yu-Chao Liu for the kind help in electrophysiological recording and morphological reconstruction. We also thank Chiu-Wen Yen, Hsiao-Han Chen, Wai-Ting Chan, and Chih-Chun Peng for various aspects of assistance.

References

Amaral, D.G., Scharfman, H.E., Lavenex, P., 2007. The dentate gyrus: fundamental neuroanatomical organization (dentate gyrus for dummies). Prog. Brain Res. 163, 3–22. http://dx.doi.org/10.1016/S0079-6123(07)63001-5.

Bean, B.P., 2009. Inhibition by an excitatory conductance: a paradox explained. Nat. Neurosci. 12 (5), 530–532. http://dx.doi.org/10.1038/nn0509-530.

Bian, F., Li, Z., Offord, J., Davis, M.D., McCormick, J., Taylor, C.P., Walker, L.C., 2006. Calcium channel alpha2-delta type 1 subunit is the major binding protein for pregabalin in neocortex, hippocampus, amygdala, and spinal cord: an ex vivo autoradiographic study in alpha2-delta type 1 genetically modified mice. Brain Res. 1075 (1), 68–80. http://dx.doi.org/10.1016/j.brainres.2005.12.084.

Brauchi, S., Orta, G., Salazar, M., Rosenmann, E., Latorre, R., 2006. A hot-sensing cold receptor: C-terminal domain determines thermosensation in transient receptor potential channels. J. Neurosci. 26 (18), 4835–4840. http://dx.doi.org/10.1523/JNEUROSCI.5080-05.2006.

Burgess, D.L., Noebels, J.L., 2000. Calcium channel defects in models of inherited generalized epilepsy. Epilepsia 41 (8), 1074–1075. http://dx.doi.org/10.1111/j.1528-1157.2000.tb00305.x.

Butt, S.J., Fuccillo, M., Nery, S., Noctor, S., Kriegstein, A., Corbin, J.G., Fishell, G., 2005. The temporal and spatial origins of cortical interneurons predict their physiological subtype. Neuron 48 (4), 591–604. http://dx.doi.org/10.1016/j.neuron.2005.09.034.

Cao, D., Ohtani, H., Ogiwara, I., Ohtani, S., Takahashi, Y., Yamakawa, K., Inoue, Y., 2012. Efficacy of stiripentol in hyperthermia-induced seizures in a mouse model of Dravet syndrome. Epilepsia 53 (7), 1140–1145. http://dx.doi.org/10.1111/j.1528-1167.2012.03497.x.

Carpenter, D.O., Alving, B.O., 1968. A contribution of an electrogenic Na + pump to membrane potential in Aplysia neurons. J. Gen. Physiol. 52 (1), 1–21.

Cheah, C.S., Yu, F.H., Westenbroek, R.E., Kalume, F.K., Oakley, J.C., Potter, G.B., Rubenstein, J.L., Catterall, W.A., 2012. Specific deletion of NaV1.1 sodium channels in inhibitory interneurons causes seizures and premature death in a mouse model of Dravet syndrome. Proc. Natl. Acad. Sci. U. S. A. 109 (36), 14646–14651. http://dx.doi.org/10.1073/pnas.1211591109.

Chen, C.Y., Tsai, M.S., Lin, C.Y., Yu, I.S., Chen, Y.T., Lin, S.R., Juan, L.W., Chen, Y.T., Hsu, H.M., Lee, L.J., Lin, S.W., 2012. Rescue of the genetically engineered Cul4b mutant mouse as a potential model for human X-linked mental retardation. Hum. Mol. Genet. 21 (19), 4270–4285. http://dx.doi.org/10.1093/hmg/dds261.

de Lanerolle, N.C., Kim, J.H., Robbins, R.J., Spencer, D.D., 1989. Hippocampal interneuron loss and plasticity in human temporal lobe epilepsy. Brain Res. 495 (2), 387–395. http://dx.doi.org/10.1016/0006-8993(89)90234-5.

Deller, T., Martinez, A., Nitsch, R., Frotscher, M., 1996. A novel entorhinal projection to the rat dentate gyrus: direct innervation of proximal dendrites and cell bodies of granule cells and GABAergic neurons. J. Neurosci. 16 (10), 3322–3333.

Depienne, C., Trouillard, O., Saint-Martin, C., Gourfinkel-An, I., Bouteiller, D., Carpentier, W., Keren, B., Abert, B., Gautier, A., Baulac, S., Arzimanoglou, A., Cazeneuve, C., Nabbout, R., LeGuern, E., 2009. Spectrum of SCN1A gene mutations associated with Dravet syndrome: analysis of 333 patients. J. Med. Genet. 46 (3), 183–191. http://dx.doi.org/10.1136/jmg.2008.062323.

Dickerson, L.W., Bonthius, D.J., Schutte, B.C., Yang, B., Barna, T.J., Bailey, M.C., Nehrke, K., Williamson, R.A., Lamb, F.S., 2002. Altered GABAergic function accompanies hippocampal degeneration in mice lacking ClC-3 voltage-gated chloride channels. Brain Res. 958 (2), 227–250. http://dx.doi.org/10.1016/S0006-8993(02)03519-9.

Duflocq, A., Le Bras, B., Bullier, E., Couraud, F., Davenne, M., 2008. Nav1.1 is predominantly expressed in nodes of Ranvier and axon initial segments. Mol. Cell. Neurosci. 39 (2), 180–192. http://dx.doi.org/10.1016/j.mcn.2008.06.008.

Dutton, S.B., Makinson, C.D., Papale, L.A., Shankar, A., Balakrishnan, B., Nakazawa, K., Escayg, A., 2012. Preferential inactivation of Scn1a in parvalbumin interneurons increases seizure susceptibility. Neurobiol. Dis. 25, 211–220. http://dx.doi.org/10.1016/j.nbd.2012.08.012.

Garrido, J.J., Giraud, P., Carlier, E., Fernandes, F., Moussif, A., Fache, M.P., Debanne, D., Dargent, B., 2003. A targeting motif involved in sodium channel clustering at the axonal initial segment. Science 300 (5628), 2091–2094. http://dx.doi.org/10.1126/science.1085167.

Gazina, E.V., Richards, K.L., Mokhtar, M.B., Thomas, E.A., Reid, C.A., Petrou, S., 2010. Differential expression of exon 5 splice variants of sodium channel alpha subunit mRNAs in the developing mouse brain. Neuroscience 166 (1), 195–200. http://dx.doi.org/10.1016/j.neuroscience.2009.12.011.

Gloyn, A.L., Diatloff-Zito, C., Edghill, E.L., Bellanné-Chantelot, C., Nivot, S., Coutant, R., Ellard, S., Hattersley, A.T., Robert, J.J., 2006. KCNJ11 activating mutations are associated with developmental delay, epilepsy and neonatal diabetes syndrome and other neurological features. Eur. J. Hum. Genet. 14 (7), 824–830. http://dx.doi.org/10.1038/sj.ejhg.5201629.

Gomez-Di Cesare, C.M., Smith, K.L., Rice, F.L., Swann, J.W., 1997. Axonal remodeling during postnatal maturation of CA3 hippocampal pyramidal neurons. J. Comp. Neurol. 384 (2), 165–180.

Gorman, A.L., Marmor, M.F., 1970. Temperature dependence of the sodium-potassium permeability ratio of a molluscan neurone. J. Physiol. 210 (4), 919–931.

Gu, F., Hazra, A., Aulakh, A., Žiburkus, J., 2014. Purinergic control of hippocampal circuit hyperexcitability in Dravet syndrome. Epilepsia 55 (2), 245–255. http://dx.doi.org/10.1111/epi.12487.

Han, S., Tai, C., Westenbroek, R.E., Yu, F.H., Cheah, C.S., Potter, G.B., Rubenstein, J.L., Scheuer, T., de la Iglesia, H.O., Catterall, W.A., 2012. Autistic-like behaviour in Scn1a+/− mice and rescue by enhanced GABA-mediated neurotransmission. Nature 489 (7416), 385–390. http://dx.doi.org/10.1038/nature11356.

Harkin, L.A., McMahon, J.M., Iona, X., Dibbens, L., Pelekanos, J.T., Zuberi, S.M., Sadleir, L.G., Andermann, E., Gill, D., Farrell, K., Connolly, M., Stanley, T., Harbord, M., Andermann, F., Wang, J., Batish, S.D., Jones, J.G., Seltzer, W.K., Gardner, A., Infantile Epileptic Encephalopathy Referral Consortium, Sutherland, G., Berkovic, S.F., Mulley, J.C., Scheffer, I.E., 2007. The spectrum of SCN1A-related infantile epileptic encephalopathies. Brain 130 (Pt3), 843–852. http://dx.doi.org/10.1093/brain/awm002.

Hernandez, C.C., Gurba, K.N., Hu, N., Macdonald, R.L., 2011. The GABRA6 mutation, R46W, associated with childhood absence epilepsy, alters 6β22 and 6β2 GABA(A) receptor channel gating and expression. J. Physiol. 589 (Pt 23), 5857–5878. http://dx.doi.org/10.1113/jphysiol.2011.218883.

Huang, H.P., Hong, C.L., Kao, C.Y., Lin, S.W., Lin, S.R., Wu, H.L., Shi, G.Y., You, L.R., Wu, C.L., Yu, I.S., 2011. Gene targeting and expression analysis of mouse Tem1/endosialin using a lacZ reporter. Gene Expr. Patterns 11 (5–6), 316–326. http://dx.doi.org/10.1016/j.gep.2011.03.001.

Ito, S., Ogiwara, I., Yamada, K., Miyamoto, H., Hensch, T.K., Osawa, M., Yamakawa, K., 2013. Mouse with Na(v)1.1 haploinsufficiency, a model for Dravet syndrome, exhibits lowered sociability and learning impairment. Neurobiol. Dis. 49, 29–40. http://dx.doi.org/10.1016/j.nbd.2012.08.003.

Jonas, P., Bischofberger, J., Fricker, D., Miles, R., 2004. Interneuron Diversity series: Fast in, fast out–temporal and spatial signal processing in hippocampal interneurons. Trends Neurosci. 27 (1), 30–40. http://dx.doi.org/10.1016/j.tins.2003.10.010.

Jou, S.B., Kao, I.F., Yi, P.L., Chang, F.C., 2013. Electrical stimulation of left anterior thalamic nucleus with high-frequency and low intensity currents reduces the rate of pilocarpine-induced epilepsy in rats. Seizure 22 (3), 221–229. http://dx.doi.org/10.1016/j.seizure.2012.12.015.

Kalume, F., Westenbroek, R.E., Cheah, C.S., Yu, F.H., Oakley, J.C., Scheuer, T., Catterall, W.A., 2013. Sudden unexpected death in a mouse model of Dravet syndrome. J. Clin. Invest. 123 (4), 1798–1808. http://dx.doi.org/10.1172/JCI66220.

Leterrier, C., Brachet, A., Dargent, B., Vacher, H., 2011. Determinants of voltage-gated sodium channel clustering in neurons. Semin. Cell Dev. Biol. 22 (2), 171–177. http://dx.doi.org/10.1016/j.semcdb.2010.09.014.

Liautard, C., Scalmani, P., Carriero, G., de Curtis, M., Franceschetti, S., Mantegazza, M., 2013. Hippocampal hyperexcitability and specific epileptiform activity in a mouse model of Dravet syndrome. Epilepsia 54 (7), 1251–1261. http://dx.doi.org/10.1111/epi.12213.

Liu, P., Jenkins, N.A., Copeland, N.G., 2003. A highly efficient recombineering-based method for generating conditional knockout mutations. Genome Res. 13 (3), 476–484. http://dx.doi.org/10.1101/gr.749203.

Liu, Y.C., Cheng, J.K., Lien, C.C., 2014. Rapid dynamic changes of dendritic inhibition in the dentate gyrus by presynaptic activity patterns. J. Neurosci. 34 (4), 1344–1357. http://dx.doi.org/10.1523/JNEUROSCI. 2566-13.2014.

Lorincz, A., Nusser, Z., 2008. Cell-type-dependent molecular composition of the axon initial segment. J. Neurosci. 28 (53), 14329–14340. http://dx.doi.org/10.1523/JNEUROSCI. 4833-08.2008.

Lothman, E.W., Stringer, J.L., Bertram, E.H., 1992. The dentate gyrus as a control point for seizures in the hippocampus and beyond. Epilepsy Res. Suppl. 7, 301–313.

Lovick, T.A., Coote, J.H., 1988. Electrophysiological properties of paraventriculo-spinal neurones in the rat. Brain Res. 454 (1–2), 123–130. http://dx.doi.org/10.1016/0006-8993(88)90810-4.

Macdonald, R.L., Kang, J.Q., Gallagher, M.J., 2012. $GABA_A$ receptor subunit mutations and genetic epilepsies. [Internet], In: Noebels, J.L., Avoli, M., Rogawski, M.A., Olsen, R.W., Delgado-Escueta, A.V. (Eds.), Source Jasper's basic mechanisms of the epilepsies, 4th edition National Center for Biotechnology Information (US), Bethesda, MD (URL http://www.ncbi.nlm.nih.gov/books/NBK98205/ (Date of last access September 2014)).

Mancardi, M.M., Striano, P., Gennaro, E., Madia, F., Paravidino, R., Scapolan, S., Dalla Bernardina, B., Bertini, E., Bianchi, A., Capovilla, G., Darra, F., Elia, M., Freri, E., Gobbi, G., Granata, T., Guerrini, R., Pantaleoni, C., Parmeggiani, A., Romeo, A., Santucci, M., Vecchi, M., Veggiotti, P., Vigevano, F., Pistorio, A., Gaggero, R., Zara, F., 2006. Familial occurrence of febrile seizures and epilepsy in severe myoclonic epilepsy of infancy (SMEI) patients with SCN1A mutations. Epilepsia 47 (10), 1629–1635. http://dx.doi.org/10.1111/j.1528-1167.2006.00641.x.

Martina, M., Schultz, J.H., Ehmke, H., Monyer, H., Jonas, P., 1998. Functional and molecular differences between voltage-gated K+ channels of fast-spiking interneurons and pyramidal neurons of rat hippocampus. J. Neurosci. 18 (20), 8111–8125.

Miller, M., 1981. Maturation of rat visual cortex. I. A quantitative study of Golgi-impregnated pyramidal neurons. J. Neurocytol. 10 (5), 859–878.
Miller, A.R., Hawkins, N.A., McCollom, C.E., Kearney, J.A., 2014. Mapping genetic modifiers of survival in a mouse model of Dravet syndrome. Genes Brain Behav. 13 (2), 163–172. http://dx.doi.org/10.1111/gbb.12099.
Mistry, A.M., Thompson, C.H., Miller, A.R., Vanoye, C.G., George Jr., A.L., Kearney, J.A., 2014. Strain- and age-dependent hippocampal neuron sodium currents correlate with epilepsy severity in Dravet syndrome mice. Neurobiol. Dis. 65, 1–11. http://dx.doi.org/10.1016/j.nbd.2014.01.006.
Ogiwara, I., Miyamoto, H., Morita, N., Atapour, N., Mazaki, E., Inoue, I., Takeuchi, T., Itohara, S., Yanagawa, Y., Obata, K., Furuichi, T., Hensch, T.K., Yamakawa, K., 2007. Nav1.1 localizes to axons of parvalbumin-positive inhibitory interneurons: a circuit basis for epileptic seizures in mice carrying an Scn1a gene mutation. J. Neurosci. 27 (22), 5903–5914. http://dx.doi.org/10.1523/JNEUROSCI. 5270-06.2007.
Ohmori, I., Hayashi, K., Wang, H., Ouchida, M., Fujita, N., Inoue, T., Michiue, H., Nishiki, T., Matsui, H., 2013. Inhalation of 10% carbon dioxide rapidly terminates Scn1a mutation-related hyperthermia-induced seizures. Epilepsy Res. 105 (1–2), 220–224. http://dx.doi.org/10.1016/j.eplepsyres.2013.01.003.
Ohno, Y., Ishihara, S., Mashimo, T., Sofue, N., Shimizu, S., Imaoku, T., Tsurumi, T., Sasa, M., Serikawa, T., 2011. Scn1a missense mutation causes limbic hyperexcitability and vulnerability to experimental febrile seizures. Neurobiol. Dis. 41 (2), 261–269. http://dx.doi.org/10.1016/j.nbd.2010.09.013.
Qiao, X., Werkman, T.R., Gorter, J.A., Wadman, W.J., van Vliet, E.A., 2013. Expression of sodium channel α subunits 1.1, 1.2 and 1.6 in rat hippocampus after kainic acid-induced epilepsy. Epilepsy Res. 106 (1–2), 17–28. http://dx.doi.org/10.1016/j.eplepsyres.2013.06.006.
Qu, L., Leung, L.S., 2008. Mechanisms of hyperthermia-induced depression of GABAergic synaptic transmission in the immature rat hippocampus. J. Neurochem. 106 (5), 2158–2169. http://dx.doi.org/10.1111/j.1471-4159.2008.05576.x.
Qu, L., Liu, X., Wu, C., Leung, L.S., 2007. Hyperthermia decreases GABAergic synaptic transmission in hippocampal neurons of immature rats. Neurobiol. Dis. 27 (3), 320–327. http://dx.doi.org/10.1016/j.nbd.2007.06.003.
Racine, R.J., 1972. Modification of seizure activity by electrical stimulation: II. Motor seizure. Electroencephalogr. Clin. Neurophysiol. 32 (3), 281–294. http://dx.doi.org/10.1016/0013-4694(72)90177-0.
Ribak, C.E., 1992. Local circuitry of GABAergic basket cells in the dentate gyrus. Epilepsy Res. Suppl. 7, 29–47.
Riva, D., Vago, C., Pantaleoni, C., Bulgheroni, S., Mantegazza, M., Franceschetti, S., 2009. Progressive neurocognitive decline in two children with Dravet syndrome, de novo SCN1A truncations and different epileptic phenotypes. Am. J. Med. Genet. A 149A (10), 2339–2345. http://dx.doi.org/10.1002/ajmg.a.33029.
Sakauchi, M., Oguni, H., Kato, I., Osawa, M., Hirose, S., Kaneko, S., Takahashi, Y., Takayama, R., Fujiwara, T., 2011. Mortality in Dravet syndrome: search for risk factors in Japanese patients. Epilepsia 52 (Suppl. 2), 50–54. http://dx.doi.org/10.1111/j.1528-1167.2011.03002.x.
Schmidt-Hieber, C., Jonas, P., Bischofberger, J., 2007. Subthreshold dendritic signal processing and coincidence detection in dentate gyrus granule cells. J. Neurosci. 27 (31), 8430–8441. http://dx.doi.org/10.1523/JNEUROSCI. 1787-07.2007.
Schuchmann, S., Schmitz, D., Rivera, C., Vanhatalo, S., Salmen, B., Mackie, K., Sipila, S.T., Voipio, J., Kaila, K., 2006. Experimental febrile seizures are precipitated by a hyperthermia-induced respiratory alkalosis. Nat. Med. 12 (7), 817–823. http://dx.doi.org/10.1038/nm1422.
Sholl, D.A., 1953. Dendritic organization in the neurons of the visual and motor cortices of the cat. J. Anat. 87 (4), 387–406.
Tai, C., Abe, Y., Westenbroek, R.E., Scheuer, T., Catterall, W.A., 2014. Impaired excitability of somatostatin- and parvalbumin-expressing cortical interneurons in a mouse model of Dravet syndrome. Proc. Natl. Acad. Sci. U. S. A. 111 (30), E3139–E3148. http://dx.doi.org/10.1073/pnas.1411131111.
Tamamaki, N., Yanagawa, Y., Tomioka, R., Miyazaki, J., Obata, K., Kaneko, T., 2003. Green fluorescent protein expression and colocalization with calretinin, parvalbumin, and somatostatin in the GAD67-GFP knock-in mouse. J. Comp. Neurol. 467 (1), 60–79. http://dx.doi.org/10.1002/cne.10905.
Tessier, C.R., Broadie, K., 2009. Activity-dependent modulation of neural circuit synaptic connectivity. Front. Mol. Neurosci. 2, 8. http://dx.doi.org/10.3389/neuro.02.008.2009.
Wang, W., Takashima, S., Segawa, Y., Itoh, M., Shi, X., Hwang, S.K., Nabeshima, K., Takeshita, M., Hirose, S., 2011. The developmental changes of Na(v)1.1 and Na(v)1.2 expression in the human hippocampus and temporal lobe. Brain Res. 1389, 61–70. http://dx.doi.org/10.1016/j.brainres.2011.02.083.
Waxman, S.G., 2007. Channel, neuronal and clinical function in sodium channelopathies: from genotype to phenotype. Nat. Neurosci. 10 (4), 405–409. http://dx.doi.org/10.1038/nn1857.
Wong, R.O., Ghosh, A., 2002. Activity-dependent regulation of dendritic growth and patterning. Nat. Rev. Neurosci. 3 (10), 803–812. http://dx.doi.org/10.1038/nrn941.
Wu, J., Fisher, R.S., 2000. Hyperthermic spreading depressions in the immature rat hippocampal slice. J. Neurophysiol. 84 (3), 1355–1360.
Yamada, K., Ji, J.J., Yuan, H., Miki, T., Sato, S., Horimoto, N., Shimizu, T., Seino, S., Inagaki, N., 2001. Protective role of ATP-sensitive potassium channels in hypoxia-induced generalized seizure. Science 292 (5521), 1543–1546. http://dx.doi.org/10.1126/science.1059829.
Yu, F.H., Mantegazza, M., Westenbroek, R.E., Robbins, C.A., Kalume, F., Burton, K.A., Spain, W.J., McKnight, G.S., Scheuer, T., Catterall, W.A., 2006. Reduced sodium current in GABAergic interneurons in a mouse model of severe myoclonic epilepsy in infancy. Nat. Neurosci. 9 (9), 1142–1149. http://dx.doi.org/10.1038/nn1754.
Zucker, R.S., 1989. Short-term synaptic plasticity. Annu. Rev. Neurosci. 12, 13–31. http://dx.doi.org/10.1146/annurev.neuro.12.1.13.